bioRxiv preprint doi: https://doi.org/10.1101/515429; this version posted January 8, 2019. The copyright holder for this preprint (which was not certified by peer review) is the author/funder, who has granted bioRxiv a license to display the preprint in perpetuity. It is made available under aCC-BY-NC-ND 4.0 International license.

Defining the dynamic chromatin landscape of nephron progenitors

Sylvia Hilliard[1], Renfang Song[1], Hongbing Liu[1], Chao-hui Chen[1], Yuwen Li[1], Melody Baddoo[2], Erik Flemington[2], Alanna Wanek[3], Jay Kolls[3], Zubaida Saifudeen[1], and Samir S. El-Dahr[1]

[1]Department of Pediatrics, Section of Pediatric Nephrology, Tulane University School of Medicine, New Orleans, LA
[2]Department of Pathology & Tulane Cancer Center, Tulane University School of Medicine, New Orleans, LA
[3]Departments of Pediatrics & Medicine, Center for Translational Research in Infection and Inflammation, Tulane University School of Medicine, New Orleans, LA

Key words: Nephrogenesis; Nephron progenitors; Chromatin

Corresponding Author:

Samir S. El-Dahr, M.D.
Department of Pediatrics
Section of Pediatric Nephrology
1430 Tulane Avenue
New Orleans, LA. 70112

(504) 988-6692
seldahr@tulane.edu

bioRxiv preprint doi: https://doi.org/10.1101/515429; this version posted January 8, 2019. The copyright holder for this preprint (which was not certified by peer review) is the author/funder, who has granted bioRxiv a license to display the preprint in perpetuity. It is made available under aCC-BY-NC-ND 4.0 International license.

Summary statement

Hilliard et al. investigated the chromatin landscape of native Six2^{+} nephron progenitors across their lifespan. They identified age-dependent changes in accessible chromatin and regulatory regions supporting the view that old nephron progenitors are epigenetically poised for differentiation.

bioRxiv preprint doi: https://doi.org/10.1101/515429; this version posted January 8, 2019. The copyright holder for this preprint (which was not certified by peer review) is the author/funder, who has granted bioRxiv a license to display the preprint in perpetuity. It is made available under aCC-BY-NC-ND 4.0 International license.

ABSTRACT

Six2^{+} cap mesenchyme cells, also called nephron progenitor cells (NPC), are precursors of all epithelial cell types of the nephron, the filtering unit of the kidney. Current evidence indicates that perinatal “old” NPC have a greater tendency to exit the progenitor niche and differentiate into nascent nephrons than their embryonic “young” counterpart. Understanding the underpinnings of NPC aging may offer insights to rejuvenate old NPC and expand the progenitor pool. Here, we compared the chromatin landscape of young and old NPC and found common features reflecting their shared lineage but also intrinsic differences in chromatin accessibility and enhancer landscape supporting the view that old NPC are epigenetically poised for differentiation. Annotation of open chromatin regions and active enhancers uncovered the transcription factor Bach2 as a potential link between the pro-renewal MAPK/AP1 and pro-differentiation Six2/b-catenin pathways that might be of critical importance in regulation of NPC fate. Our data provide the first glimpse of the dynamic chromatin landscape of NPC and serve as a platform for future studies of the impact of genetic or environmental perturbations on the epigenome of NPC.

bioRxiv preprint doi: https://doi.org/10.1101/515429; this version posted January 8, 2019. The copyright holder for this preprint (which was not certified by peer review) is the author/funder, who has granted bioRxiv a license to display the preprint in perpetuity. It is made available under aCC-BY-NC-ND 4.0 International license.

INTRODUCTION

Reciprocal interactions between the ureteric bud and surrounding NPC of the cap mesenchyme govern nephron induction. The cap mesenchyme is composed of an early progenitor Cited1^{+}/Six2^{+} compartment and a transit Cited1^{-}/Six2^{+} compartment that subsequently differentiate into the pretubular aggregate, the precursor of the renal vesicle, the earliest epithelial precursor of the nephron (Brown et al., 2013; Mugford et al., 2009). Careful morphometric studies and cell cycle analyses have shown that the proportion of NPC progressing through the cell cycle decreases with NPC aging, whereas the contribution of cell death is minimal, suggesting that all NPC exit occurs via differentiation into early nephrons (Short et al., 2014). Using genetic and primary cell culture models, Fgf9 and Bmp7 were shown to stimulate the MAPK pathway activation of Fos and Jun in the cap mesenchyme leading to the formation of the AP-1 heterodimer which stimulates cell cycle and growth factor genes contributing to the maintenance of the NPC population (Muthukrishnan et al., 2015). Although Fgf9 levels do not fall appreciably during NPC aging, Fgf20 levels do (Barak et al., 2012). It is therefore possible that reduced growth factor availability/activity in the niche is partly responsible for the short lifespan of NPC. However, there are also intrinsic differences between young and old NPC. For example, Six2 (and other stemness factors such as Wt1, Osr1 and Sall1) levels decline in postnatal NPC suggesting that these low levels cannot sustain NPC stemness in the face of elevated canonical Wnt signaling. A decline in the glycolytic capacity has also been shown by RNA-seq on postnatal NPC (Chen et al., 2015) as well as in primary young and old NPC (Liu et al., 2017). These changes translate into differences in cell behavior as demonstrated in the heterochronic transplantation studies (Chen et al., 2015): whereas young NPC tend to remain in the progenitor niche, old NPC exit and differentiate. The biological underpinnings of NPC aging, i.e., the greater tendency of perinatal NPC to differentiate compared to their embryonic counterpart, are not well understood.

Here, we compared the chromatin landscape of young and old NPC and find that dynamic chromatin accessibility to developmental enhancers is an intrinsic property of aging NPC. Genome-wide ATAC-seq and ChIP-seq uncovered common and

bioRxiv preprint doi: https://doi.org/10.1101/515429; this version posted January 8, 2019. The copyright holder for this preprint (which was not certified by peer review) is the author/funder, who has granted bioRxiv a license to display the preprint in perpetuity. It is made available under aCC-BY-NC-ND 4.0 International license.

differentially accessible chromatin regions in young vs. old NPC reflecting their shared identity but also their maturational differences. Relative gain and loss of enhancer accessibility correlated with NPC gene expression and identified the poised epigenetic state of differentiation genes. While the open chromatin of young NPC is enriched in binding sites for the core NPC transcription factors (Six2, Wt1, Hoxa/c/d, Tead, AP1), old NPC gain chromatin accessibility to the Bach2/Batf complex, a repressor of AP1-mediated transcriptional activation. Importantly, Bach2 is a component of the transcription factor code of the renal vesicle, the earliest precursor of the nephron, and is a genomic target of the Six2/b-catenin complex, whereas MAPK/AP1 is required to maintain the progenitor state of NPC. In summary, our data support the notion that dynamic changes in the NPC epigenome over their lifespan balance NPC proliferation and differentiation. We propose Bach2 as a potential molecular link between the MAPK/AP1 and Six2/b-catenin pathways.

bioRxiv preprint doi: https://doi.org/10.1101/515429; this version posted January 8, 2019. The copyright holder for this preprint (which was not certified by peer review) is the author/funder, who has granted bioRxiv a license to display the preprint in perpetuity. It is made available under aCC-BY-NC-ND 4.0 International license.

RESULTS

Experimental protocol (Fig. 1)

To compare the open chromatin landscape of young (embryonic) and old (perinatal) NPC, we applied the assay for transposase-accessible chromatin by high-throughput sequencing (ATAC-seq) to fluorescence-activated cell sorted (FACS) GFP^+ cells isolated from embryonic (E13, E16) and perinatal (P0, P2) $Six2^{GC}$ mice (Kobayashi et al., 2008), which specifically express GFP under the Six2 regulatory elements in the cap mesenchyme. By gating fluorescence and forward scatter, we also obtained enriched populations of GFP^{high} and GFP^{low} NPC from newborn mice (referred to as P0-H and P0-L), representing undifferentiated and differentiating NPC, respectively. To reduce background, remove mitochondria from the transposition reaction, and increase the complexity of the library, we used the Omni-ATAC protocol (Corces et al., 2017) on 50,000 FACS-GFP^+ (n=3-4 biological replicates per age group). In another set of experiments, we applied magnetic-activated cell sorting (MACS) (Brown et al., 2013) to isolate the NPC from E13 and P0 CD-1 mice. To enrich for the self-renewing NPC population, E13 and P0 MACS-NPC were expanded in nephron progenitor expansion medium (NPEM) (Brown et al., 2013; Brown et al., 2015) for two passages then subjected to chromatin immunoprecipitation.

Assessment of NPC diversity

We applied droplet-based single-cell RNA sequencing to 10,524 GFP^+ cells isolated from E16 $Six2^{GC}$ mice. Clustering analysis identified 13 distinct cell clusters varying from as few as 150 cells to as many as 1616 cells per cluster (Fig. 2A). Cluster 2 and Clusters 6-8 were enriched in NPC expressing centrosome duplication, cell cycle and DNA replication genes (Fig. 2B). Cluster 12 contained fewer numbers of NPC (343 cells, 3%) and expressed early differentiation genes such as *Wnt4, Pax8, Wfdc2 and Kdm2b* (Fig. 2C). This was not surprising since lower levels of Six2(GFP) continue to be present in early nascent elements such as the pretubular aggregate and renal vesicle. As discussed later in the text (Fig 7A), chromatin profiling of E13 and P0 NPC confirmed that the promoters of these early differentiation genes are bivalent

bioRxiv preprint doi: https://doi.org/10.1101/515429; this version posted January 8, 2019. The copyright holder for this preprint (which was not certified by peer review) is the author/funder, who has granted bioRxiv a license to display the preprint in perpetuity. It is made available under aCC-BY-NC-ND 4.0 International license.

(H3K4me1/H3K27me3) and therefore in a poised transcriptional state expressing low transcript levels. Cluster 13 is composed of NPC co-expressing stromal mesenchymal markers such as Lgals1, Maged2, and Gpc3 (Fig. 2D). A previously published study using scRNA-seq showed that individual NPC exhibit stochastic expression of stroma markers (Brunskill et al., 2014). These findings confirm that $Six2^{+}$ NPC are composed of diverse cell populations some which are actively engaged in self-renewal while others are poised to differentiate.

The open chromatin landscape of NPC

ATAC-seq results were highly reproducible between biological replicates and showed a clear enrichment at the regulatory elements. As an example (Fig. 3A), in the *Six2* locus, the replicates show that the open chromatin regions are concentrated in the promoter region and the annotated enhancer located 60kb upstream of the TSS (Park et al., 2012). Analysis of ATAC-seq peaks revealed that young NPC possessed more distal open chromatin regions than older NPC (Fig. 3B). Heatmap clustering of ATAC peaks in annotated genes around the TSS (-1 to +1 kb) did not reveal significant differences in open chromatin in E16 and P2 NPC (Fig. 3C). Gene Ontology of the distal (-1 to -60 kb) regions showed common and distinct gene signature sets and pathways associated with the open chromatin regions in E16 and P2 NPC (Fig. 3D). Among the common features are regulation of stem cell maintenance and nephrogenesis as well as Notch signaling and the TCA cycle. Distinct functional signatures include response to reactive oxygen species and pentose phosphate pathway (E16 NPC) and regulation of cell shape and ATP synthesis (P2 NPC).

NPC aging is associated with differential chromatin accessibility

We compared the open chromatin regions of E16 and P2 NPC as well as of P0-H and P0-L NPC using DiffBind R (http://bioconductor.org/packages/release/bioc/vignettes/DiffBind/inst/doc/DiffBind.pdf). The affinity analysis is a quantitative approach to assess for differential chromatin access at consensus peaks. This method takes read densities computed over consensus peak regions and provides a statistical estimate of the difference in read concentration between

bioRxiv preprint doi: https://doi.org/10.1101/515429; this version posted January 8, 2019. The copyright holder for this preprint (which was not certified by peer review) is the author/funder, who has granted bioRxiv a license to display the preprint in perpetuity. It is made available under aCC-BY-NC-ND 4.0 International license.

the two conditions. Heatmap correlation plots, Principal Component Analysis, and MA plots highlight the differences in ATAC read concentrations between E16 and P2 NPC and P0-H and P0-L NPC (Fig. 4 A-C, F-H). The MA plots, shown in Fig. 4 C,H depict the differences between ATAC signals in the two experimental samples by transforming the data onto M (log ratio) and A (mean average) scales, then plotting these values. Differential chromatin accessibility depicted in the MA plots is expressed as a log fold change of at least 2-fold and a p-value of < 0.05. The MA plot in Fig. 4C shows the relative gain of open chromatin regions in E16 NPC (above the 0 threshold line) as compared to the gain in P2 NPC (below the 0 threshold line). The MA plot in Fig. 4H depicts the relative gain of open chromatin regions in P0-H (above the 0-threshold line) as compared to the gain in P0-L NPC (below the 0-threshold line). NPC aging is associated with a decline in differential chromatin accessibility of the stemness factor, *Six2*, but a reciprocal increase in chromatin accessibility to the differentiation transcription factor *HNF1-b* (Fig. 4 D,E). Likewise, differentiating P0-L NPC gain chromatin accessibility in differentiation genes (e.g., Lef1, Irx, Hnf1b, Tcf7l2 and some of the Notch components) (Fig. 4 I). P0-L NPC also displayed increased accessibility around the TSS as compared to P0-H NPC (Fig. 4 J). Collectively, these findings illustrate the dynamic open chromatin landscape of NPC during maturation and are consistent with the view that old NPC are epigenetically programmed to differentiate.

ATAC peaks correlate with NPC gene expression and transcription factor binding

We also compared our ATAC-seq signals representing open promoters and enhancers with published gene expression of NPC lineage (O'Brien et al., 2018). The results showed that progenitor genes in E16 NPC (e.g., Six2, Osr1 and Meox1) exhibit more open chromatin at distal elements and promoters than P2 NPC (Fig. 5A). In comparison, poised genes in P2 NPC (e.g., Wnt4, Sulf1 and Mafb) exhibit more open chromatin features than E16 NPC (Fig. 5A). These findings indicate a good correlation between chromatin accessibility and gene expression levels during NPC aging.

The open chromatin regions indicated by the ATAC peaks also correlated with the ChIP-seq peaks representing active enhancers (H3K4me1/H3K27ac) – this study - as

bioRxiv preprint doi: https://doi.org/10.1101/515429; this version posted January 8, 2019. The copyright holder for this preprint (which was not certified by peer review) is the author/funder, who has granted bioRxiv a license to display the preprint in perpetuity. It is made available under aCC-BY-NC-ND 4.0 International license.

well as with binding sites of the NPC core transcription factors Six2, Osr1 and Wt1 – previously shown by O'Brien et al. (O'Brien et al., 2018) (Fig. 5B). Of interest, we found that the binding of Hdac1 was a reliable indicator of open chromatin at the promoter region of actively transcribed genes where rapid cycles of histone acetylation and deacetylation are required for resetting the chromatin of active genes (Wang et al., 2009) (Fig. 5B).

NPC chromatin profiles in genes implicated in renal function

We examined the ATAC signature of genes found in genome-wide association studies of estimated glomerular filtration rate and demonstrate preferential mapping of variants to regulatory regions in kidney but not extra-renal tissues (Pattaro et al., 2016). Although many of these genes were not active in NPC, they displayed open chromatin regions and were marked by H3K4me1 on putative primed enhancers (Fig. 5C). The homeobox transcription factor, *UNCX,* showed broad open chromatin regions that increase in width with NPC aging and is bivalent in E16 NPC but active in P2 NPC (Fig. 5C).

The histone modifications landscape of pro-renewal and differentiation pathways

Given that the niche microenvironment (growth factor availability) may not be similar in native young vs. old NPC, we examined the epigenetic states of MACS-isolated E13 and P0 NPC grown in NPEM for two passages. The MACS isolation, which is performed on wild-type tissue, also avoids the Six2GFPCre transgene, in case it had a non-specific effect on the chromatin landscape. ChIP-seq analysis was then performed to map active (H3K4me1/H3K27ac), repressed (H3K27me3) and poised (H3K4me1/H3K27me3) enhancers. Fig S1 A-D depicts that pro-renewal pathway genes (Akt signaling, cell cycle, RTK signaling, and epigenetic regulators) are all decorated with active histone marks, the exception being cell cycle inhibitors which are occupied by broad regions of the repressive mark H3K27me3 (Fig S1B). In comparison, Fig. 6A shows that genes required for mesenchyme-to-epithelium transition are occupied by bivalent chromatin regions (H3K4me1/K27me3) indicating they are silent but poised for transcription. Furthermore, poised differentiation genes showed a decrease in occupancy in the repressive H3K27me3 mark and a reciprocal gain of H3K27ac with NPC aging (Fig.

bioRxiv preprint doi: https://doi.org/10.1101/515429; this version posted January 8, 2019. The copyright holder for this preprint (which was not certified by peer review) is the author/funder, who has granted bioRxiv a license to display the preprint in perpetuity. It is made available under aCC-BY-NC-ND 4.0 International license.

6 A,B). Finally, non-lineage genes, e.g., pro-neural developmental genes, are occupied by broad domains of H3K27me3 which serve to restrain their expression (Fig. 6C).

Collectively, these results indicate that young and old NPC exhibit intrinsic differences in chromatin accessibility and histone modifications at annotated and putative promoters and enhancers.

Chromatin profiling links the transcription factor Bach2 with NPC aging

We used ATAC-seq to identify transcription factor motifs within the accessible distal regions in young and old NPC. HOMER revealed enrichment of the DNA-binding motifs of the master NPC transcription factors Six2 and Wt1 across all age groups reflecting their shared lineage (Table 1 and Fig S2). Hoxc9 and Tead DNA-binding motifs were also enriched among the top 21 most enriched motifs. Hoxa11 and Hoxd11 motifs, on the other hand, were enriched in young E13 NPC but not older NPC. Notably, binding motifs for AP-1, BATF and especially Bach2 were progressively more enriched in older and differentiating NPC (Table 1 and Fig S2).

Using ChIP-seq, we identified 18692 primed enhancers (marked by H3K4me1) at E13 compared to 27983 primed enhancers at P0 (P0>E13 +1.5-fold) (Fig. 7A). The numbers of H3K27ac-marked active enhancers were 3333 at E13 and 16207 at P0 (P0>E13 +4.8-fold) (Fig. 7B). Motif enrichment analysis of E13 NPC revealed that among the 15 most enriched active enhancers were the core factors AP1, Sox4, Hoxc9, Hoxd11 and Six2 (Fig. 7C). At P0, the 15 most enriched active enhancers were the core TFs plus Pax8, Batf, Rbpj, AP1 and Bach2 (Fig. 7D). Together, the ATAC and ChIP data highlight the age-related enrichment of Bach2/Batf motifs suggesting a temporal association between age-related changes in chromatin accessibility and the binding of AP1/Bach2/Batf.

Bach2 (BTB domain and CNC Homolog 2) is a transcription factor that is enriched in immune cells and plays a key role in regulation of the developmental B-cell transcriptional programs (Zhou et al., 2016) . Previous studies have shown that Bach2 acts by recruiting Batf and competes with AP-1 for sequence-specific DNA binding on

bioRxiv preprint doi: https://doi.org/10.1101/515429; this version posted January 8, 2019. The copyright holder for this preprint (which was not certified by peer review) is the author/funder, who has granted bioRxiv a license to display the preprint in perpetuity. It is made available under aCC-BY-NC-ND 4.0 International license.

target genes (Kuwahara et al., 2016; Roychoudhuri et al., 2016). Importantly, our scRNA-seq indicates that Bach2 is expressed in the NPC along with Batf and the AP1 components Junb and Atf3 (Fig. 8A). Furthermore, interrogation of the GUDMAP/RBK database revealed that *Bach2* is expressed in the distal part of the renal vesicle, the earliest nephron precursor (Fig. 8B). ATAC and ChIP-seq also showed the presence of two putative regulatory elements in the *Bach2* gene marked by the presence of consensus ATAC/H3K27ac/Six2/b-catenin peaks (Fig. 8C), suggesting that *Bach2* is a genomic target of canonical Wnt signaling, the principal driver of NPC differentiation.

bioRxiv preprint doi: https://doi.org/10.1101/515429; this version posted January 8, 2019. The copyright holder for this preprint (which was not certified by peer review) is the author/funder, who has granted bioRxiv a license to display the preprint in perpetuity. It is made available under aCC-BY-NC-ND 4.0 International license.

DISCUSSION

Understanding the epigenetic mechanisms governing the nephron progenitor life span (Adli et al., 2015) is of great translational importance, since low nephron number predisposes to hypertension and chronic kidney disease later in life. Importantly, monogenic mutations account for only about 20% of all cases of abnormal kidney development. Accordingly, there is a critical gap in our knowledge of how adverse prenatal environmental events affect renal development in the offspring. Moreover, a better understanding of the physiological, metabolic and epigenetic underpinnings of NPC aging may open new avenues to expand the nephron progenitor pool.

We previously interrogated the histone signatures of cultured metanephric mesenchyme cell lines (McLaughlin et al., 2013) and found that the onset of differentiation is accompanied by resolution of chromatin bivalency conforming to prior observations in pluripotent cells wherein genes essential for lineage commitment carry permissive histone modifications and appear poised for differentiation. In these studies, we observed that Wnt-responsive differentiation genes gain β-catenin/H3K4me3 binding and lose H3K27me3 at the TCF/LEF binding sites. By contrast, the promoters of progenitor genes show a gain of repressive marks and the loss of the active histone marks. Interestingly, immunolocalization studies in developing kidneys revealed that Six2+ nephron progenitors have higher levels of the repressive H3K9me2 and H3K27me3 marks and the histone modifiers, G9a, Ezh2 and HDACs (Liu et al., 2018; McLaughlin et al., 2014). While these studies were informative, additional work was needed to clarify whether the dynamic chromatin landscape observed in metanephric mesenchyme cell lines applies to native NPC.

In the present study, using native freshly isolated NPC across their lifespan, we demonstrate that as the NPC age in the niche, chromatin accessibility to the regulatory regions of poised differentiation genes increases, likely preparing these gene networks for activation of the epithelial nephrogenesis program. These changes are not simply the results of changing proportions of the self-renewing and differentiating NPC populations but likely intrinsic, since young and old NPC grown in the same growth factor expansion

bioRxiv preprint doi: https://doi.org/10.1101/515429; this version posted January 8, 2019. The copyright holder for this preprint (which was not certified by peer review) is the author/funder, who has granted bioRxiv a license to display the preprint in perpetuity. It is made available under aCC-BY-NC-ND 4.0 International license.

medium also show significant differences in their chromatin enhancer landscape. We speculate that these maturational changes in chromatin accessibility are likely orchestrated by concomitant changes in the epigenetic machinery such as the Polycomb complex, ATP-dependent chromatin remodelers, DNA methylation and the NuRD/HDAC complex, that govern the access of master regulators to their cis-acting elements. Indeed, there is genetic evidence that perturbations of the epigenetic machinery disrupt the balance between NPC proliferation and differentiation in vivo (Denner and Rauchman, 2013; El-Dahr and Saifudeen, 2018; Liu et al., 2018; Zhang et al., 2018).

A new finding of this study is that NPC aging is associated with enhanced accessibility at the Bach2/Batf occupancy sites. As mentioned earlier in the text, Bach2 was identified as part of the transcription factor signature of the distal renal vesicle, a compartment that receives high levels of Wnt9b/ß-catenin signaling (Brunskill et al., 2014). This leads us to the following working model (Fig. 8D). In young NPC, Six2/co-repressor complexes inhibit *Bach2* transcription. With further activation of Wnt/ß-catenin signaling and concomitant decline in Six2 levels, the Six2/TCF repressor is replaced by ß-catenin/TCF/co-activator complex leading to induction of *Bach2* transcription. The Bach2/Batf complex subsequently displaces the AP-1 complex inhibiting expression of AP1 targets (e.g., cell cycle genes). It is also conceivable that Bach2 targets differentiation genes to activate them. To our knowledge, studies of renal development have not been reported in Bach2- or Bach1/Bach2-deficient mice. Future investigations of *Bach2* function in nephrogenesis and delineation of Bach2-target genes will shed light on some of these gene regulatory networks. If indeed Bach2 links the proliferation and differentiation pathways in the NPC, targeting Bach2 may be a useful tool to manipulate the fate and lifespan of the NPC in renal regenerative medicine.

bioRxiv preprint doi: https://doi.org/10.1101/515429; this version posted January 8, 2019. The copyright holder for this preprint (which was not certified by peer review) is the author/funder, who has granted bioRxiv a license to display the preprint in perpetuity. It is made available under aCC-BY-NC-ND 4.0 International license.

MATERIALS AND METHODS

Isolation of NPC

NPC were isolated from E13.5, E16.5, P0 and P2 CD1 mice or *Six2GFPCre* mice by magnetic-activated cell sorting (MACS) (Brown et al., 2015) or fluorescent-activated cell sorting (FACS). Animal protocols utilized in this study were approved by and in strict adherence to guidelines established by the Tulane University Institutional Animal Care and Use Committee.

ATAC-seq

For sample library preparation we followed the Omni-ATAC method outlined by (Buenrostro et al., 2015; Corces et al., 2017). Briefly 50,000 nuclei from FACS-sorted cells were processed for Tn5 transposase-mediated tagmentation and adaptor incorporation at sites of accessible chromatin. This reaction was carried out using the Nextera DNA Library Prep kit (FC-121-1030, Illumina) at 37°C for 30min. Following tagmentation the DNA fragments were purified using the Zymo DNA Clean and Concentrator Kit (D4014, ZYMO Research). Library amplification was performed using the Ad1 and any of Ad2.1through Ad2.12 barcoded primers (Buenrostro et al., 2015). The quality of the purified DNA library was assessed on 6%TBE gels as well as on a Bioanalyzer (2100 Expert software, Agilent Technologies) using High Sensitivity DNA Chips (5067-4626, Agilent Technologies Inc.). The appropriate concentration of sample was determined using the Qubit Fluorometer (Molecular Probes). Four nM samples were pooled and run on a NextSeq 500/550 Hi Output Kit (20024907, Illumina, Inc. San Diego, CA) and the NextSeq 500 Illumina Sequencer to obtain paired end reads of 75bp. Three to four independent biological replicates were sequenced per sample.

Read processing and normalization of data

The paired-end reads for each sample run across 4 lanes of the flow cell (20022408, Illumina) were concatenated to obtain one forward and one reverse fastq.gz files each. The quality of the reads was assessed using FASTQC (v0.11.7). The paired end reads were aligned to the mouse reference genome mm10 using Bowtie 2. The properly aligned reads were filtered for mitochondrial reads (Sam tools) and cleared of duplicates (Picard-

bioRxiv preprint doi: https://doi.org/10.1101/515429; this version posted January 8, 2019. The copyright holder for this preprint (which was not certified by peer review) is the author/funder, who has granted bioRxiv a license to display the preprint in perpetuity. It is made available under aCC-BY-NC-ND 4.0 International license.

tools, v1.77). Only paired reads with high mapping quality (MAPQ >30) were included in the downstream analysis. The narrow peaks were called using MACS2 using the following parameters (effective genome size = 1.87e+09; - -nomodel -p 0.001 - - no lambda; band width = 300, d = 200; p value cut off = 1.00e-03). Normalized bigwig files were generated using bedtools. Annotation and Known as well as de novo Motif discovery was achieved with Hypergeometric Optimization of Motif Enrichment (HOMER). Gene ontology analysis was performed using GREAT analysis 3.0. Heatmaps, density plots and differentially mapped regions were generated using DiffBind (Bioconductor).

Single Cell RNA-seq

We performed gene expression profiling of approximately 10,000 individual cells by using 10x Single Cell RNAseq technique provided by 10x Genomics. We first obtained a single cell suspension where cell viability was 88% or higher. These cells were applied for GEM generation and barcoding using the manufacturer's protocol. 10x™ GemCode™ Technology allows the partition of thousands of cells into nanoliter-scale Gel Bead-In-EMulsions (GEMs) with application of ~750,000 barcodes to separately index each cell's transcriptome. After GEM reaction mixture, full-length barcoded cDNA were generated and amplified by PCR to generate sufficient mass for library construction. Following enzymatic fragmentation, end-repair, A-tailing, and adaptor ligation, indexed libraries were generated and sequenced. We used Cell Ranger version 2.1.1 (10x Genomics) to process raw sequencing data and Seurat suite version 2.2.1 for downstream analysis. Filtering was performed to remove multiplets and broken cells and uninteresting sources of variation were regressed out. Variable genes were determined by iterative selection based on the dispersion vs. average expression of the gene. For clustering, principal-component analysis was performed for dimension reduction. Top 10 principal components (PCs) were selected by using a permutation-based test implemented in Seurat and passed to t-SNE for visualization of clusters.

ChIP-seq

Chromatin was prepared from E13.5 and P0 NPC using the Diagenode iDeal ChIP-seq kit for Histones. Samples corresponding to 0.5 million cells were resuspended in 100 μl

bioRxiv preprint doi: https://doi.org/10.1101/515429; this version posted January 8, 2019. The copyright holder for this preprint (which was not certified by peer review) is the author/funder, who has granted bioRxiv a license to display the preprint in perpetuity. It is made available under aCC-BY-NC-ND 4.0 International license.

of shearing buffer iS1 and sheared during 8 cycles of 30 seconds “ON” / 30 seconds “OFF” with the Bioruptor Pico combined with the Bioruptor Water cooler. The shearing efficiency was analyzed using an automated capillary electrophoresis system Fragment Analyzer (High sensitivity NGS fragment kit) after RNAse treatment, reversal of the crosslinking and purification of DNA. Based on optimization conditions, we used optimal antibody quantity resulting in higher enrichment and lower background (1 µg each of anti-H3K4me1, anti-H3K27me3 and anti-H3K27ac). The antibodies used were the following: H3K27ac (Diagenode antibody, C15410196, lot A1723-0041D), H3K4me1 (Diagenode antibody, C15410194, lot A1862D), H3K27me3 (Diagenode antibody, C15410195, lot A1811-001P) . H3K4me3 (Diagenode antibody, C15410003, lot 5051-001P) was used as a ChIP Positive Control. After the IP, immunoprecipitated DNA was analyzed by qPCR to evaluate the specificity of the reaction. The primers pair, Six2 Prom (Fwd3 _ Rev 4) was used as positive control for the H3K27ac mark, Mouse Negative Control Primer Set1 (Commercially available from Active Motif) was used as negative control region. Myogenic differentiation antigen 1 9MYOD1) and Mouse Negative Control Primer Set 3 were respectively used as positive and negative control regions for the H3K27me3 mark. Finally, Paired box 8 (Pax8int) and Mouse Negative Control Set 1 were respectively used as positive and negative controls for H3K4me1 mark. An IP with a control isotype (IgG 1 µg) was also performed. 500 pg of DNA was subsequently used for library preparation using the MicroPlex v2 protocol. The ChIP samples (8 samples in total) were processed together. A control library was processed in parallel of the samples using the same amount of a control Diagenode ChIP’s DNA. According to the protocol, 12 cycles of amplification were performed to amplify the libraries. After amplification, 1 µl of each library was loaded on BioAnalyzer for quality and quantified using the Qubit ds DNA HS kit. Reference genomes were obtained from the UCSC genome browser. Sequencing was performed on an Illumina HiSeq 2500, running HiSeq Control Software 2.2.58. Quality control of sequencing reads was performed using FastQC. Reads were then aligned to the reference genome using BWA v. 0.7.5a. Samples were filtered for regions blacklisted by the ENCODE project. Subsequently samples were deduplicated using SAMtools v. 1.3.1. Alignment coordinates were converted to BED format using BEDTools v.2.17 and peak calling was performed using Sicer. The main ChIP-Seq statistics are

bioRxiv preprint doi: https://doi.org/10.1101/515429; this version posted January 8, 2019. The copyright holder for this preprint (which was not certified by peer review) is the author/funder, who has granted bioRxiv a license to display the preprint in perpetuity. It is made available under aCC-BY-NC-ND 4.0 International license.

shown in Supplemental Table S2. Peaks sets generated with peak calling analysis were analyzed using DiffBind R/Bioconductor package.

bioRxiv preprint doi: https://doi.org/10.1101/515429; this version posted January 8, 2019. The copyright holder for this preprint (which was not certified by peer review) is the author/funder, who has granted bioRxiv a license to display the preprint in perpetuity. It is made available under aCC-BY-NC-ND 4.0 International license.

Acknowledgments

The Authors are grateful to Kejing Song (Tulane Genomic and epigenomic and sequencing cores), and the laboratory of Dr. Mazhar Adli (University of Virginia) for help in the early phase of the study.

Competing interests

No competing interests declared.

Funding

This work was supported by NIH grant DK114500 (SED) and the Louisiana Board of Regents Endowed Chairs for Eminent Scholars program (JKK).

Data availability

The files have been deposited in NCBI GSE124804.

bioRxiv preprint doi: https://doi.org/10.1101/515429; this version posted January 8, 2019. The copyright holder for this preprint (which was not certified by peer review) is the author/funder, who has granted bioRxiv a license to display the preprint in perpetuity. It is made available under aCC-BY-NC-ND 4.0 International license.

REFERENCES

Adli, M., Parlak, M., Li, Y., El-Dahr, S.S., 2015. Epigenetic States of nephron progenitors and epithelial differentiation. J Cell Biochem 116, 893-902.

Barak, H., Huh, S.H., Chen, S., Jeanpierre, C., Martinovic, J., Parisot, M., Bole-Feysot, C., Nitschke, P., Salomon, R., Antignac, C., Ornitz, D.M., Kopan, R., 2012. FGF9 and FGF20 maintain the stemness of nephron progenitors in mice and man. Dev Cell 22, 1191-1207.

Brown, A.C., Muthukrishnan, S.D., Guay, J.A., Adams, D.C., Schafer, D.A., Fetting, J.L., Oxburgh, L., 2013. Role for compartmentalization in nephron progenitor differentiation. Proc Natl Acad Sci U S A 110, 4640-4645.

Brown, A.C., Muthukrishnan, S.D., Oxburgh, L., 2015. A synthetic niche for nephron progenitor cells. Dev Cell 34, 229-241.

Brunskill, E.W., Park, J.S., Chung, E., Chen, F., Magella, B., Potter, S.S., 2014. Single cell dissection of early kidney development: multilineage priming. Development 141, 3093-3101.

Buenrostro, J.D., Wu, B., Chang, H.Y., Greenleaf, W.J., 2015. ATAC-seq: A Method for Assaying Chromatin Accessibility Genome-Wide. Curr Protoc Mol Biol 109, 21 29 21-29.

Chen, S., Brunskill, E.W., Potter, S.S., Dexheimer, P.J., Salomonis, N., Aronow, B.J., Hong, C.I., Zhang, T., Kopan, R., 2015. Intrinsic Age-Dependent Changes and Cell-Cell Contacts Regulate Nephron Progenitor Lifespan. Dev Cell 35, 49-62.

Corces, M.R., Trevino, A.E., Hamilton, E.G., Greenside, P.G., Sinnott-Armstrong, N.A., Vesuna, S., Satpathy, A.T., Rubin, A.J., Montine, K.S., Wu, B., Kathiria, A., Cho, S.W., Mumbach, M.R., Carter, A.C., Kasowski, M., Orloff, L.A., Risca, V.I., Kundaje, A., Khavari, P.A., Montine, T.J., Greenleaf, W.J., Chang, H.Y., 2017. An improved ATAC-seq protocol reduces background and enables interrogation of frozen tissues. Nat Methods 14, 959-962.

Denner, D.R., Rauchman, M., 2013. Mi-2/NuRD is required in renal progenitor cells during embryonic kidney development. Dev Biol 375, 105-116.

El-Dahr, S.S., Saifudeen, Z., 2018. Epigenetic regulation of renal development. Semin Cell Dev Biol.

Kobayashi, A., Valerius, M.T., Mugford, J.W., Carroll, T.J., Self, M., Oliver, G., McMahon, A.P., 2008. Six2 defines and regulates a multipotent self-renewing nephron progenitor population throughout mammalian kidney development. Cell Stem Cell 3, 169-181.

Kuwahara, M., Ise, W., Ochi, M., Suzuki, J., Kometani, K., Maruyama, S., Izumoto, M., Matsumoto, A., Takemori, N., Takemori, A., Shinoda, K., Nakayama, T., Ohara, O., Yasukawa, M., Sawasaki, T., Kurosaki, T., Yamashita, M., 2016. Bach2-Batf interactions control Th2-type immune response by regulating the IL-4 amplification loop. Nat Commun 7, 12596.

Liu, H., Chen, S., Yao, X., Li, Y., Chen, C.H., Liu, J., Saifudeen, Z., El-Dahr, S.S., 2018. Histone deacetylases 1 and 2 regulate the transcriptional programs of nephron progenitors and renal vesicles. Development 145.

Liu, J., Edgington-Giordano, F., Dugas, C., Abrams, A., Katakam, P., Satou, R., Saifudeen, Z., 2017. Regulation of Nephron Progenitor Cell Self-Renewal by Intermediary Metabolism. J Am Soc Nephrol 28, 3323-3335.

McLaughlin, N., Wang, F., Saifudeen, Z., El-Dahr, S.S., 2014. In situ histone landscape of nephrogenesis. Epigenetics 9, 222-235.

bioRxiv preprint doi: https://doi.org/10.1101/515429; this version posted January 8, 2019. The copyright holder for this preprint (which was not certified by peer review) is the author/funder, who has granted bioRxiv a license to display the preprint in perpetuity. It is made available under aCC-BY-NC-ND 4.0 International license.

McLaughlin, N., Yao, X., Li, Y., Saifudeen, Z., El-Dahr, S.S., 2013. Histone signature of metanephric mesenchyme cell lines. Epigenetics 8, 970-978.
Mugford, J.W., Yu, J., Kobayashi, A., McMahon, A.P., 2009. High-resolution gene expression analysis of the developing mouse kidney defines novel cellular compartments within the nephron progenitor population. Dev Biol 333, 312-323.
Muthukrishnan, S.D., Yang, X., Friesel, R., Oxburgh, L., 2015. Concurrent BMP7 and FGF9 signalling governs AP-1 function to promote self-renewal of nephron progenitor cells. Nat Commun 6, 10027.
O'Brien, L.L., Guo, Q., Bahrami-Samani, E., Park, J.S., Hasso, S.M., Lee, Y.J., Fang, A., Kim, A.D., Guo, J., Hong, T.M., Peterson, K.A., Lozanoff, S., Raviram, R., Ren, B., Fogelgren, B., Smith, A.D., Valouev, A., McMahon, A.P., 2018. Transcriptional regulatory control of mammalian nephron progenitors revealed by multi-factor cistromic analysis and genetic studies. PLoS Genet 14, e1007181.
Park, J.S., Ma, W., O'Brien, L.L., Chung, E., Guo, J.J., Cheng, J.G., Valerius, M.T., McMahon, J.A., Wong, W.H., McMahon, A.P., 2012. Six2 and Wnt regulate self-renewal and commitment of nephron progenitors through shared gene regulatory networks. Dev Cell 23, 637-651.
Pattaro, C., Teumer, A., Gorski, M., Chu, A.Y., Li, M., Mijatovic, V., Garnaas, M., Tin, A., Sorice, R., Li, Y., Taliun, D., Olden, M., Foster, M., Yang, Q., Chen, M.H., Pers, T.H., Johnson, A.D., Ko, Y.A., Fuchsberger, C., Tayo, B., Nalls, M., Feitosa, M.F., Isaacs, A., Dehghan, A., d'Adamo, P., Adeyemo, A., Dieffenbach, A.K., Zonderman, A.B., Nolte, I.M., van der Most, P.J., Wright, A.F., Shuldiner, A.R., Morrison, A.C., Hofman, A., Smith, A.V., Dreisbach, A.W., Franke, A., Uitterlinden, A.G., Metspalu, A., Tonjes, A., Lupo, A., Robino, A., Johansson, A., Demirkan, A., Kollerits, B., Freedman, B.I., Ponte, B., Oostra, B.A., Paulweber, B., Kramer, B.K., Mitchell, B.D., Buckley, B.M., Peralta, C.A., Hayward, C., Helmer, C., Rotimi, C.N., Shaffer, C.M., Muller, C., Sala, C., van Duijn, C.M., Saint-Pierre, A., Ackermann, D., Shriner, D., Ruggiero, D., Toniolo, D., Lu, Y., Cusi, D., Czamara, D., Ellinghaus, D., Siscovick, D.S., Ruderfer, D., Gieger, C., Grallert, H., Rochtchina, E., Atkinson, E.J., Holliday, E.G., Boerwinkle, E., Salvi, E., Bottinger, E.P., Murgia, F., Rivadeneira, F., Ernst, F., Kronenberg, F., Hu, F.B., Navis, G.J., Curhan, G.C., Ehret, G.B., Homuth, G., Coassin, S., Thun, G.A., Pistis, G., Gambaro, G., Malerba, G., Montgomery, G.W., Eiriksdottir, G., Jacobs, G., Li, G., Wichmann, H.E., Campbell, H., Schmidt, H., Wallaschofski, H., Volzke, H., Brenner, H., Kroemer, H.K., Kramer, H., Lin, H., Leach, I.M., Ford, I., Guessous, I., Rudan, I., Prokopenko, I., Borecki, I., Heid, I.M., Kolcic, I., Persico, I., Jukema, J.W., Wilson, J.F., Felix, J.F., Divers, J., Lambert, J.C., Stafford, J.M., Gaspoz, J.M., Smith, J.A., Faul, J.D., Wang, J.J., Ding, J., Hirschhorn, J.N., Attia, J., Whitfield, J.B., Chalmers, J., Viikari, J., Coresh, J., Denny, J.C., Karjalainen, J., Fernandes, J.K., Endlich, K., Butterbach, K., Keene, K.L., Lohman, K., Portas, L., Launer, L.J., Lyytikainen, L.P., Yengo, L., Franke, L., Ferrucci, L., Rose, L.M., Kedenko, L., Rao, M., Struchalin, M., Kleber, M.E., Cavalieri, M., Haun, M., Cornelis, M.C., Ciullo, M., Pirastu, M., de Andrade, M., McEvoy, M.A., Woodward, M., Adam, M., Cocca, M., Nauck, M., Imboden, M., Waldenberger, M., Pruijm, M., Metzger, M., Stumvoll, M., Evans, M.K., Sale, M.M., Kahonen, M., Boban, M., Bochud, M., Rheinberger, M., Verweij, N., Bouatia-Naji, N., Martin, N.G., Hastie, N., Probst-Hensch, N., Soranzo, N., Devuyst, O., Raitakari, O., Gottesman, O., Franco, O.H., Polasek, O., Gasparini, P., Munroe, P.B., Ridker, P.M., Mitchell, P., Muntner, P., Meisinger, C., Smit, J.H., Consortium, I.,

bioRxiv preprint doi: https://doi.org/10.1101/515429; this version posted January 8, 2019. The copyright holder for this preprint (which was not certified by peer review) is the author/funder, who has granted bioRxiv a license to display the preprint in perpetuity. It is made available under aCC-BY-NC-ND 4.0 International license.

Consortium, A., Cardiogram, Group, C.H.-H.F., Consortium, E.C., Kovacs, P., Wild, P.S., Froguel, P., Rettig, R., Magi, R., Biffar, R., Schmidt, R., Middelberg, R.P., Carroll, R.J., Penninx, B.W., Scott, R.J., Katz, R., Sedaghat, S., Wild, S.H., Kardia, S.L., Ulivi, S., Hwang, S.J., Enroth, S., Kloiber, S., Trompet, S., Stengel, B., Hancock, S.J., Turner, S.T., Rosas, S.E., Stracke, S., Harris, T.B., Zeller, T., Zemunik, T., Lehtimaki, T., Illig, T., Aspelund, T., Nikopensius, T., Esko, T., Tanaka, T., Gyllensten, U., Volker, U., Emilsson, V., Vitart, V., Aalto, V., Gudnason, V., Chouraki, V., Chen, W.M., Igl, W., Marz, W., Koenig, W., Lieb, W., Loos, R.J., Liu, Y., Snieder, H., Pramstaller, P.P., Parsa, A., O'Connell, J.R., Susztak, K., Hamet, P., Tremblay, J., de Boer, I.H., Boger, C.A., Goessling, W., Chasman, D.I., Kottgen, A., Kao, W.H., Fox, C.S., 2016. Genetic associations at 53 loci highlight cell types and biological pathways relevant for kidney function. Nat Commun 7, 10023.

Roychoudhuri, R., Clever, D., Li, P., Wakabayashi, Y., Quinn, K.M., Klebanoff, C.A., Ji, Y., Sukumar, M., Eil, R.L., Yu, Z., Spolski, R., Palmer, D.C., Pan, J.H., Patel, S.J., Macallan, D.C., Fabozzi, G., Shih, H.Y., Kanno, Y., Muto, A., Zhu, J., Gattinoni, L., O'Shea, J.J., Okkenhaug, K., Igarashi, K., Leonard, W.J., Restifo, N.P., 2016. BACH2 regulates CD8(+) T cell differentiation by controlling access of AP-1 factors to enhancers. Nat Immunol 17, 851-860.

Short, K.M., Combes, A.N., Lefevre, J., Ju, A.L., Georgas, K.M., Lamberton, T., Cairncross, O., Rumballe, B.A., McMahon, A.P., Hamilton, N.A., Smyth, I.M., Little, M.H., 2014. Global quantification of tissue dynamics in the developing mouse kidney. Dev Cell 29, 188-202.

Wang, Z., Zang, C., Cui, K., Schones, D.E., Barski, A., Peng, W., Zhao, K., 2009. Genome-wide mapping of HATs and HDACs reveals distinct functions in active and inactive genes. Cell 138, 1019-1031.

Zhang, L., Ettou, S., Khalid, M., Taglienti, M., Jain, D., Jung, Y.L., Seager, C., Liu, Y., Ng, K.H., Park, P.J., Kreidberg, J.A., 2018. EED, a member of the polycomb group, is required for nephron differentiation and the maintenance of nephron progenitor cells. Development 145.

Zhou, Y., Wu, H., Zhao, M., Chang, C., Lu, Q., 2016. The Bach Family of Transcription Factors: A Comprehensive Review. Clin Rev Allergy Immunol 50, 345-356.

bioRxiv preprint doi: https://doi.org/10.1101/515429; this version posted January 8, 2019. The copyright holder for this preprint (which was not certified by peer review) is the author/funder, who has granted bioRxiv a license to display the preprint in perpetuity. It is made available under aCC-BY-NC-ND 4.0 International license.

Table 1.

Ranking of top transcription factor motifs in ATAC-seq open chromatin peaks within the distal upstream regions (-1 to -60 kb of TSS). Rank range: 1-21.

Motif	E13	E16	P0-H	P0-L	P2
Six2	3	3	3	2	3
Hoxc9	5	9	5	13	13
Wt1	14	20	9	14	15
Tead	9	5	12	19	18
Hoxa11	15	>21	>21	>21	>21
Hoxd11	16	>21	>21	>21	>21
AP1	>21	18	15	10	10
Batf	>21	17	10	11	8
Batf	>21	>21	>21	21	14

Supplemental Table 1: Statistics of ChIP-seq data.

Sample	Total reads	Uniquely aligned	Mapping efficiency	Peaks
E13.5 H3K4me1	54,619,120	39,237,983	0.7184	80,698
E13.5 H3K27me3	56,249,415	38,580,490	0.6859	5,949
E13.5 H3K27ac	64,813,226	38,273,136	0.5905	44,127
P0 H3K4me1	61,563,165	40,930,218	0.6640	77,947
P0 H3K27me3	65,761,659	39,721,356	0.6040	5,510
P0 H3K27ac	68,768,975	33,936,258	0.4935	27,442

FIGURE LEGENDS

Figure 1. Experimental strategy for epigenetic and transcriptional profiling of nephron progenitor cells (NPC).

Figure 2. Single cell RNA-seq reveals NPC diversity. NPC from E16 *Six2GFPCre* mice were isolated by FACS and subjected to droplet-based scRNA-seq (10X Genomics platform). (A) Unbiased clustering of GFP-positive Six2-lineage NPC analyzed by single-cell RNA-seq. (B-D) Gene expression plots for marker genes; cluster numbers as indicated.

Figure 3. Profiling of open chromatin regions in young and old NPC by ATAC-seq reveals common and distinct biological features. (A) Representative ATAC-seq profiles of biological replicates from young (E13, E16) and old (P0, P2) NPC. P0-H and P0-L represent GFP^{high} and GFP^{low} perinatal NPC. (B) Total numbers of ATAC-seq peaks separated into promoter ($\pm$1kb transcription start site) and distal genomic regions (-1 to -60 kb) in NPC of various ages. (C) Heatmap of ATAC peaks in the -1 to +1 kb around TSS in annotated genes at E16 and P2 NPC. (D) Functional annotation of ATAC peaks by GREAT analysis in young and old NPC.

Figure 4. Differential chromatin accessibility in young and old NPC. Heatmap (A,F), Principal Component Analysis (B, G) and MA plot (C,H) of ATAC-seq peaks in E16 vs. P2 NPC or P0-H vs. P0-L NPC. (D,E) Differential chromatin accessibility at the *Six2* and HNF1b locus between E16 vs. P2 NPC. (I) Differential chromatin accessibility upon differentiation between P0-H and P0-L NPC. (J) Heatmap of ATAC peaks in the -1 to +1 kb around TSS in annotated genes at E16 and P2 NPC.

Figure 5. Open chromatin profiles correlate with gene expression and transcription factor binding at annotated and putative enhancers of NPC developmental regulators. (A) ATAC-seq and RNA-seq of progenitor and differentiation genes at E16.5 and P2 NPC. (B) IGV tracks showing integration of ATAC-seq and ChIP-seq peaks in

promoters and enhancers of the progenitor genes, *Osr1*, *Gas1* and *Gdnf*. (C) ATAC/ChIP signature of genes found in genome-wide association studies of estimated glomerular filtration rate to demonstrate preferential mapping of associated variants to regulatory regions in kidney but not extra-renal tissues (Pattaro et al., 2016).

Figure 6. ChIP-seq profiling of histone modifications in poised differentiation (A,B) and non-lineage proneural (C) genes in young and old NPC.

Figure 7. ChIP-seq of E13 and P0 NPC grown in NPC expansion medium reveals age-related gain of enhancers and confirms enrichment with AP1, Bach2 and AP1 motifs. (A,B) Venn diagrams of unique and shared H3K4me1 and H3K27ac active regions. Affinity binding analysis performed on the shared regions reveals a net gain of enhancers in P0 NPC. (C) HOMER analysis at E13 and P0 active enhancers defines distinct sets of enriched motifs in E13 and P0 NPC.

Figure 8. The transcription factor, *Bach2*, is expressed in the early differentiating nephron epithelium and displays active enhancers bound by Six2/β-catenin. (A) scRNA showing expression of *Bach2/Batf* transcripts and AP1 components in NPC. (B) *in situ* hybridization in TS23 stage developing mouse kidney showing that *Bach2* is expressed specifically in the pretubular aggregate (PTA) and distal renal vesicle (RV) (Source: Gudmap.org). (C) IGV tracks of the *Bach2* locus: note age-related opening of chromatin in the distal upstream region of *Bach2* (small arrow). These peaks are congruent with binding of ChIP-seq peaks for Six2 and β-catenin at two active enhancer elements (boxed regions). (D) A transcriptional model for chromatin state transition during the NPC lifespan. In young NPC, Bach2 (a differentiation-promoting gene) is repressed by Six2/Tcf, whereas genes involved in stemness maintenance are activated by the growth factor/AP1 signaling module. As the NPC ages, Six2 levels decline and canonical Wnt activity is enhanced leading to Bach2 induction. Bach2/Batf in turn competes for DNA binding with the AP1 complex to turn off expression of renewal genes.

Supplemental Figure 1. ChIP-seq profiling of histone modifications in representative active pro-renewal genes in young and old NPC.

Supplemental Figure 2. Motif enrichment analysis of ATAC-seq footprints identifies distinct sets of transcription factor binding sites in aging NPC. Binding motifs for the core transcription factors (Six2/Wt1/Hoxd11/Tead) are enriched in NPC of all ages reflecting their shared lineage identity. Open chromatin regions of aging NPC tend to be enriched in binding motifs for AP-1/Bach2/Batf.

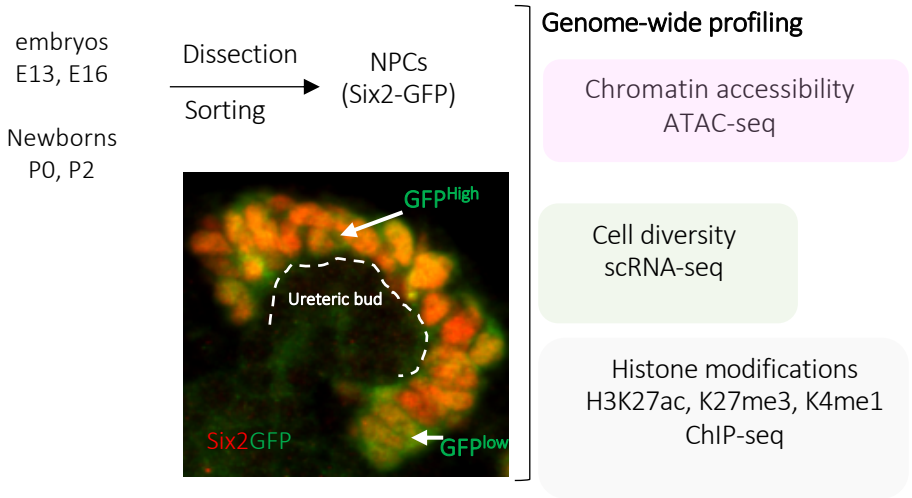
embryos
E13, E16
Newborns
P0, P2
Dissection
Sorting
NPCs
(Six2-GFP)
GFPHigh
Ureteric bud
Six2GFP
GFPlow
Genome-wide profiling
Chromatin accessibility
ATAC-seq
Cell diversity
scRNA-seq
Histone modifications
H3K27ac, K27me3, K4me1
ChIP-seq

Fig. 1

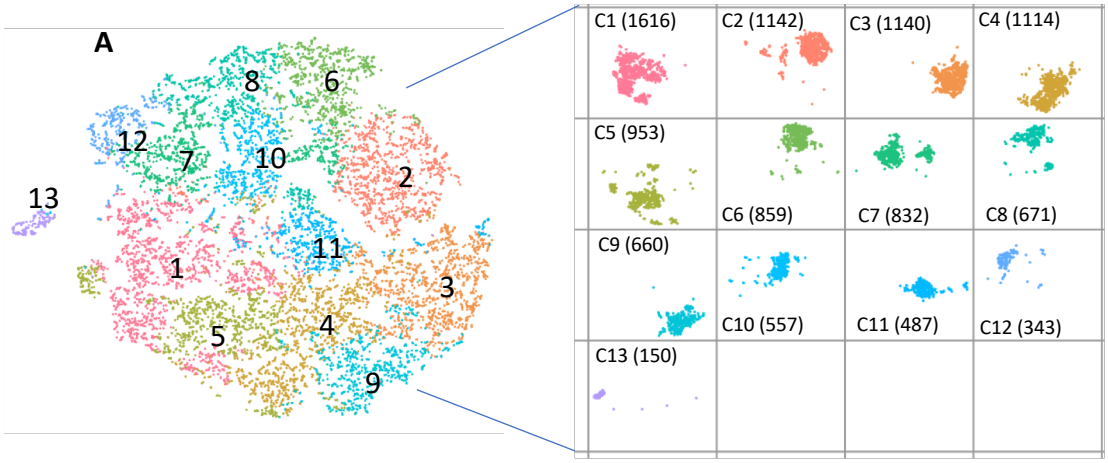

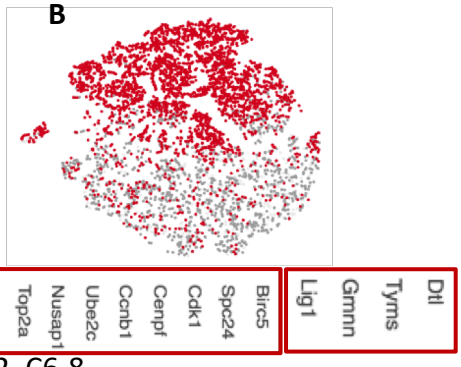

C2, C6-8
centrosome duplication
Cell cycle
DNA replication

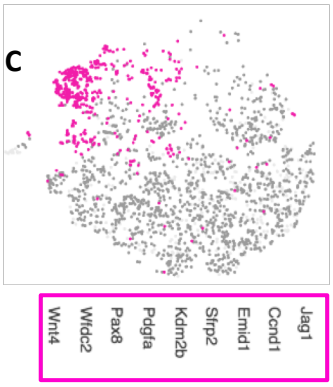

C12
Differentiation

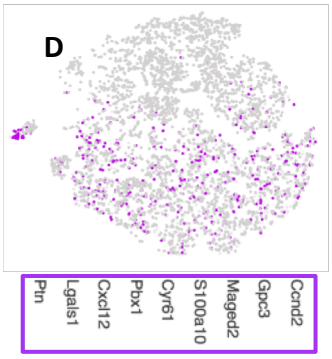

C13
Cell-matrix binding
Chemokine signaling
Stroma

Fig. 2

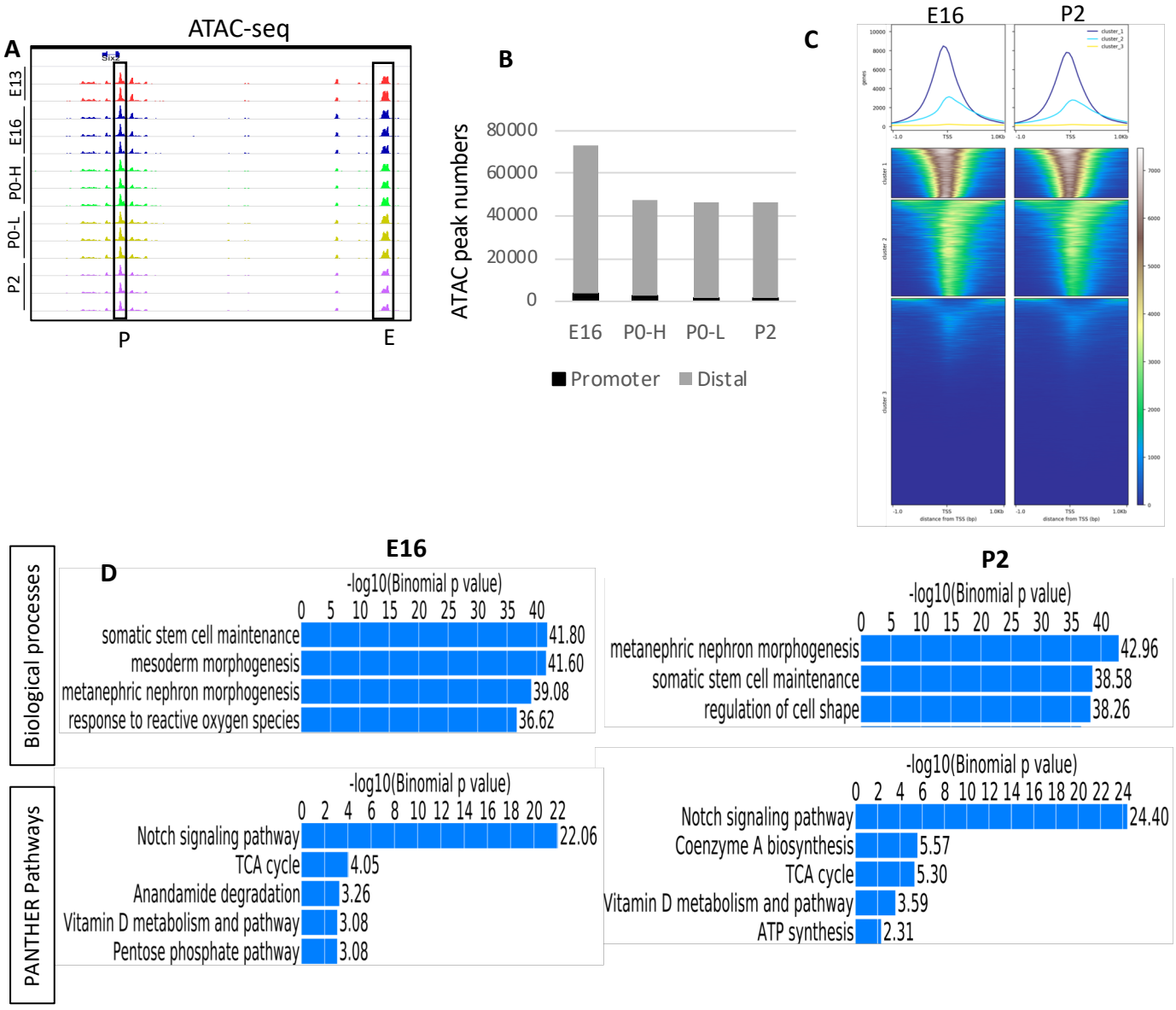
A
ATAC-seq
E13
E16
P0-H
P0-L
P2
P
E
B
ATAC peak numbers
80000
60000
40000
20000
0
E16
P0-H
P0-L
P2
Promoter
Distal
C
E16
P2
D
Biological processes
E16
-log10(Binomial p value)
0 5 10 15 20 25 30 35 40
somatic stem cell maintenance 41.80
mesoderm morphogenesis 41.60
metanephric nephron morphogenesis 39.08
response to reactive oxygen species 36.62
P2
-log10(Binomial p value)
0 5 10 15 20 25 30 35 40
metanephric nephron morphogenesis 42.96
somatic stem cell maintenance 38.58
regulation of cell shape 38.26
PANTHER Pathways
-log10(Binomial p value)
0 2 4 6 8 10 12 14 16 18 20 22
Notch signaling pathway 22.06
TCA cycle 4.05
Anandamide degradation 3.26
Vitamin D metabolism and pathway 3.08
Pentose phosphate pathway 3.08
-log10(Binomial p value)
0 2 4 6 8 10 12 14 16 18 20 22 24
Notch signaling pathway 24.40
Coenzyme A biosynthesis 5.57
TCA cycle 5.30
Vitamin D metabolism and pathway 3.59
ATP synthesis 2.31

Fig. 3

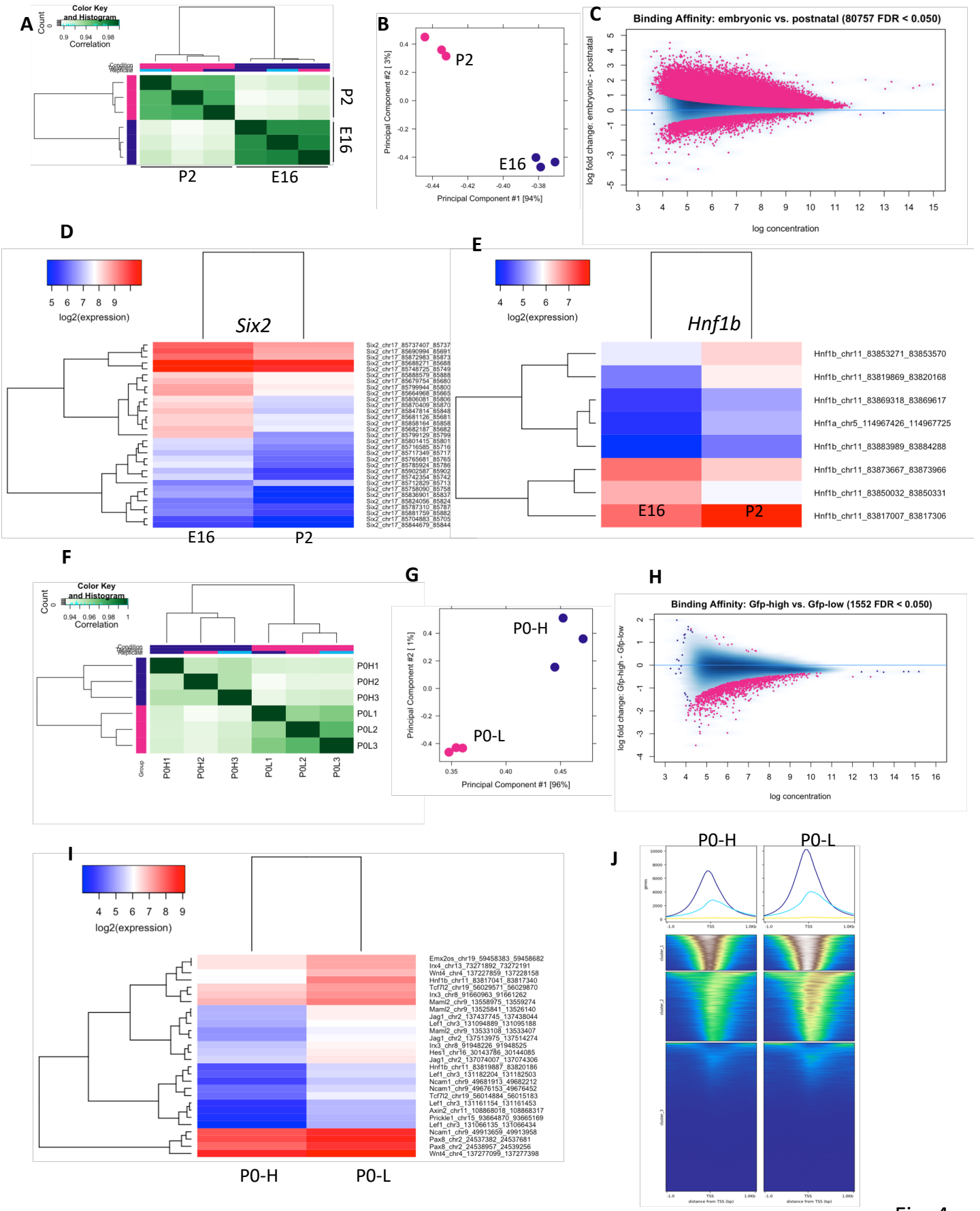
A
Color Key and Histogram
Count
Correlation
P2
E16
B
Principal Component #2 [3%]
Principal Component #1 [94%]
C
Binding Affinity: embryonic vs. postnatal (80757 FDR < 0.050)
log fold change: embryonic - postnatal
log concentration
D
log2(expression)
Six2
E16
P2
E
log2(expression)
Hnf1b
Hnf1b_chr11_83853271_83853570
Hnf1b_chr11_83819869_83820168
Hnf1b_chr11_83869318_83869617
Hnf1a_chr5_114967426_114967725
Hnf1b_chr11_83883989_83884288
Hnf1b_chr11_83873667_83873966
Hnf1b_chr11_83850032_83850331
Hnf1b_chr11_83817007_83817306
E16
P2
F
Color Key and Histogram
Count
Correlation
P0H1
P0H2
P0H3
P0L1
P0L2
P0L3
Group
G
Principal Component #2 [1%]
Principal Component #1 [96%]
P0-H
P0-L
H
Binding Affinity: Gfp-high vs. Gfp-low (1552 FDR < 0.050)
log fold change: Gfp-high - Gfp-low
log concentration
I
log2(expression)
Emx2os_chr19_59458383_59458682
Irx4_chr13_73271892_73272191
Wnt4_chr4_137227859_137228158
Hnf1b_chr11_83817041_83817340
Tcf7l2_chr19_56029571_56029870
Irx3_chr8_91660963_91661262
Maml2_chr9_13558975_13559274
Maml2_chr9_13525841_13526140
Jag1_chr2_137437745_137438044
Lef1_chr3_131094889_131095188
Maml2_chr9_13533108_13533407
Jag1_chr2_137513975_137514274
Irx3_chr8_91948226_91948525
Hes1_chr16_30143786_30144085
Jag1_chr2_137074007_137074306
Hnf1b_chr11_83819887_83820186
Lef1_chr3_131182204_131182503
Ncam1_chr9_49681913_49682212
Ncam1_chr9_49676153_49676452
Tcf7l2_chr19_56014884_56015183
Lef1_chr3_131161154_131161453
Axin2_chr11_108868018_108868317
Prickle1_chr15_93664870_93665169
Lef1_chr3_131066135_131066434
Ncam1_chr9_49913659_49913958
Pax8_chr2_24537382_24537681
Pax8_chr2_24538957_24539256
Wnt4_chr4_137277099_137277398
P0-H
P0-L
J
P0-H
P0-L
cluster_1
cluster_2
cluster_3
TSS
distance from TSS (bp)

Fig. 4

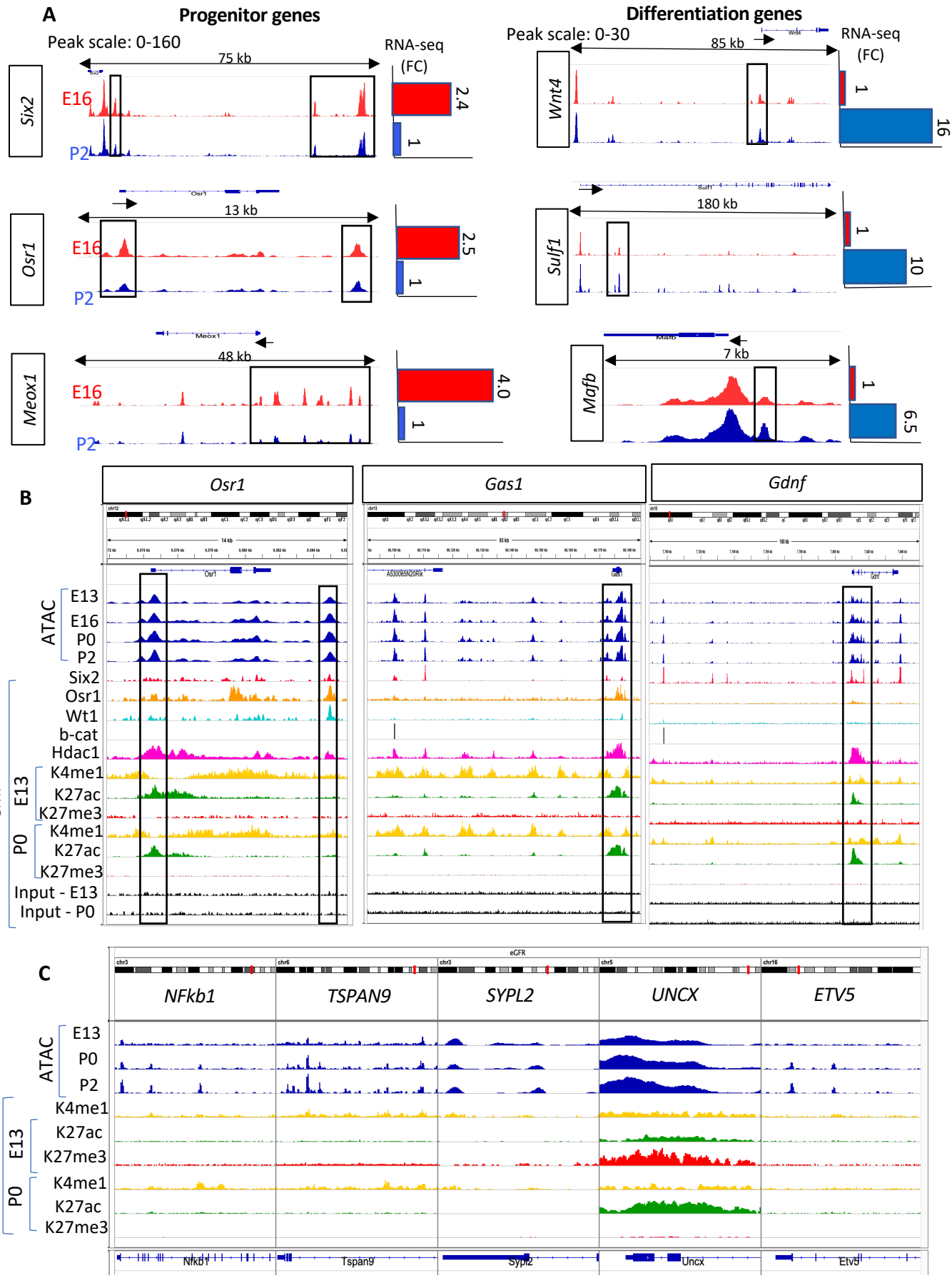
A
Progenitor genes
Peak scale: 0-160
75 kb
RNA-seq (FC)
Six2
E16
P2
2.4
1
13 kb
Osr1
2.5
48 kb
Meox1
4.0
Differentiation genes
Peak scale: 0-30
85 kb
Wnt4
16
180 kb
Sulf1
10
7 kb
Mafb
6.5
B
Osr1
Gas1
Gdnf
ATAC
E13
E16
P0
P2
ChIP
Six2
Osr1
Wt1
b-cat
Hdac1
K4me1
K27ac
K27me3
Input - E13
Input - P0
C
NFkb1
TSPAN9
SYPL2
UNCX
ETV5
Nfkb1
Tspan9
Sypl2
Uncx
Etv5

Fig. 5

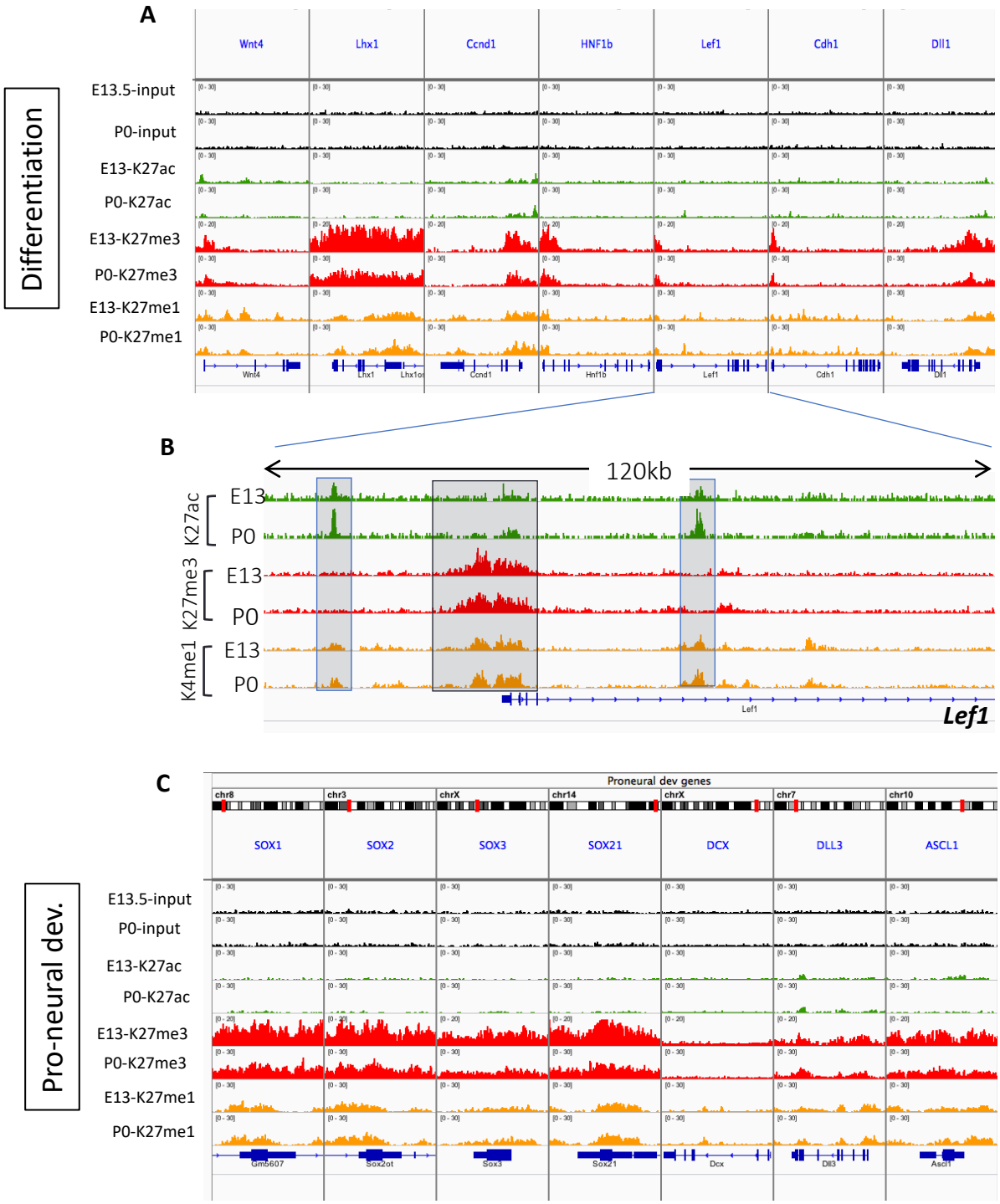
A
Differentiation
Wnt4
Lhx1
Ccnd1
HNF1b
Lef1
Cdh1
Dll1
E13.5-input
P0-input
E13-K27ac
P0-K27ac
E13-K27me3
P0-K27me3
E13-K27me1
P0-K27me1
B
120kb
K27ac
K27me3
K4me1
E13
P0
Lef1
C
Pro-neural dev.
Proneural dev genes
chr8
chr3
chrX
chr14
chrX
chr7
chr10
SOX1
SOX2
SOX3
SOX21
DCX
DLL3
ASCL1
E13.5-input
P0-input
E13-K27ac
P0-K27ac
E13-K27me3
P0-K27me3
E13-K27me1
P0-K27me1
Gm5607
Sox2ot
Sox3
Sox21
Dcx
Dll3
Ascl1

Fig. 6

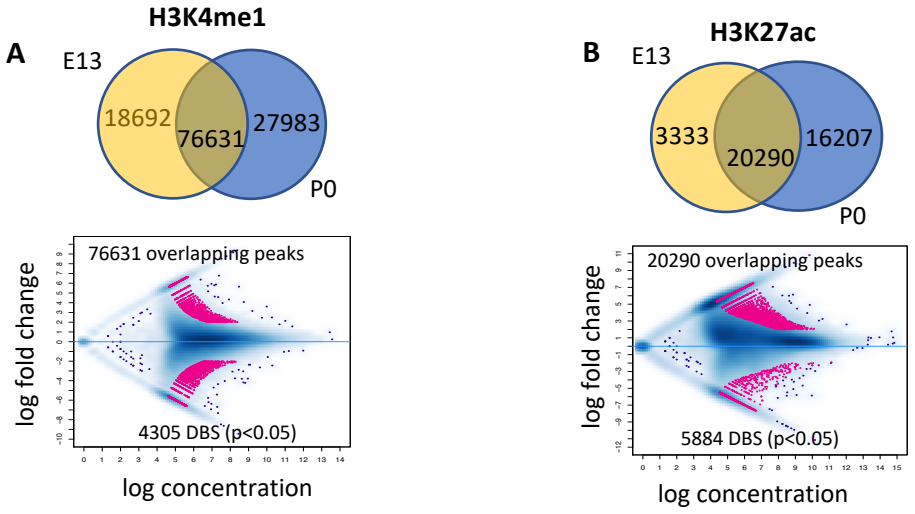

C

H3K4me1/H3K27ac
E13

	Name	P-value	#Target sequences with Motif	% of Targets Sequences with Motif
	AP1	1e-198	1097	5.87%
	Sox4	1e-6	1754	9.38%
	Hoxc9	1e-180	1830	9.79%
	Hoxd11	1e-49	3025	16.18%
	Six2	1e-52	776	4.15%

D

H3K4me1/H3K27ac
P0

	Name	P-value	#Target sequences with Motif	% of Targets Sequences with Motif
	Pax8	1e-428	10412	6.27%
	Batf	1e-43	2363	6.4%
	Rbpj	1e-14	3337	14.16%
	AP-1	1e-61	1590	6.75%
	Bach2	1e-39	828	2.24%

Fig. 7

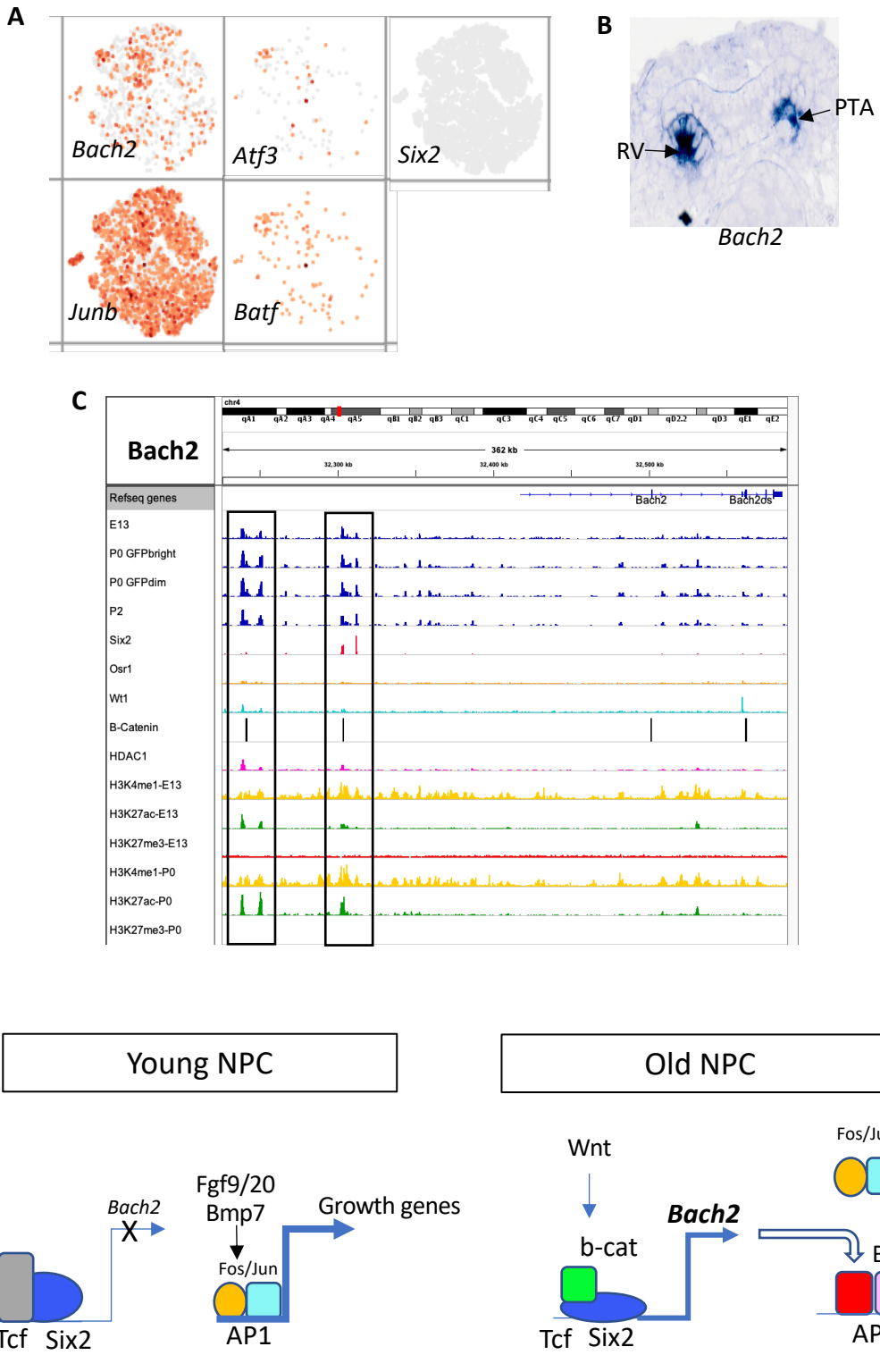
A
Bach2
Atf3
Six2
Junb
Batf
B
PTA
RV
Bach2
C
Bach2
362 kb
Refseq genes
E13
P0 GFPbright
P0 GFPdim
P2
Six2
Osr1
Wt1
B-Catenin
HDAC1
H3K4me1-E13
H3K27ac-E13
H3K27me3-E13
H3K4me1-P0
H3K27ac-P0
H3K27me3-P0
D
Young NPC
Old NPC
Bach2
X
Tcf
Six2
Fgf9/20
Bmp7
Fos/Jun
AP1
Growth genes
Wnt
b-cat
Bach2
Fos/Jun
Batf
AP1
Growth genes
X

Fig. 8

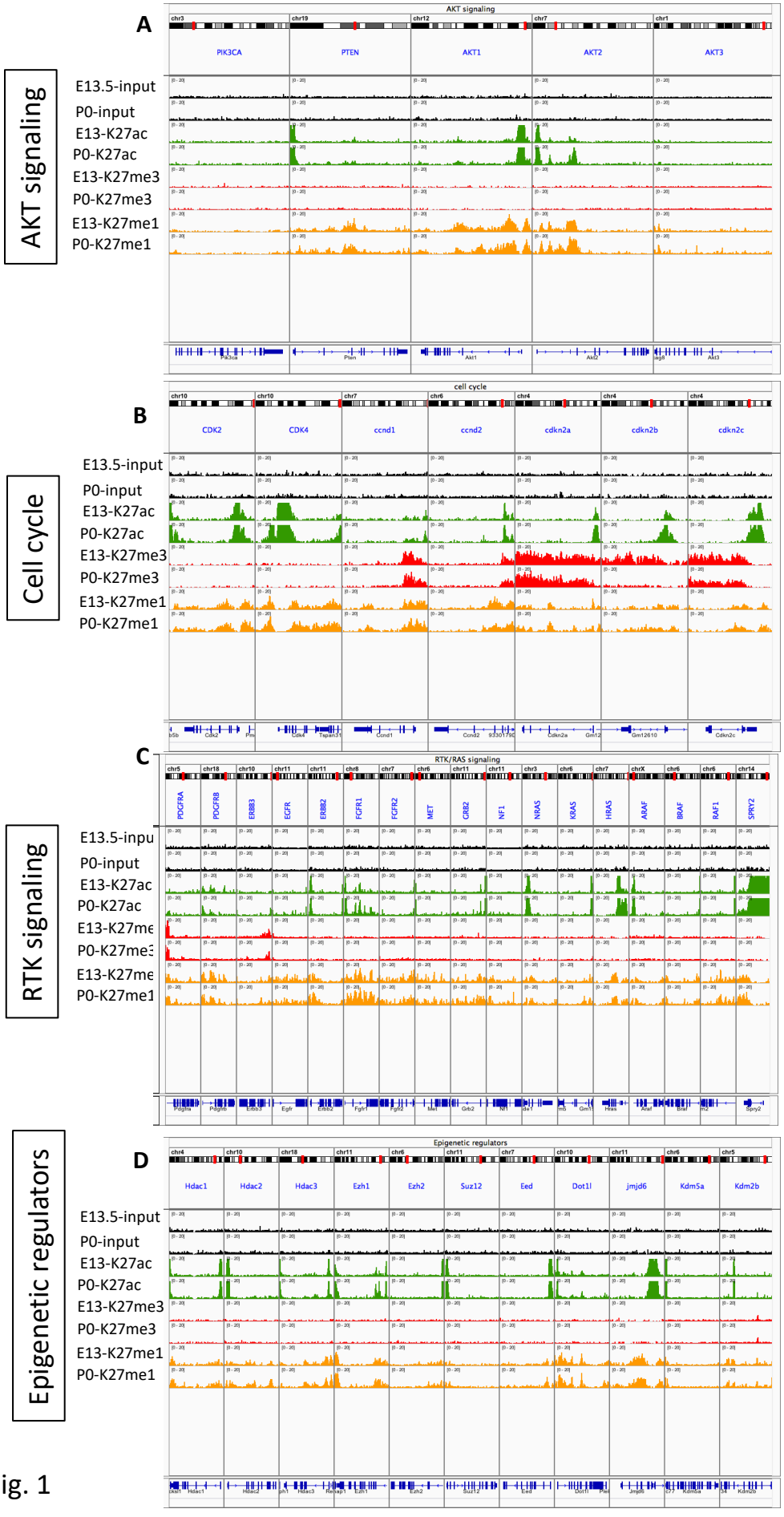
A
AKT signaling
PIK3CA
PTEN
AKT1
AKT2
AKT3
E13.5-input
P0-input
E13-K27ac
P0-K27ac
E13-K27me3
P0-K27me3
E13-K27me1
P0-K27me1
B
cell cycle
CDK2
CDK4
ccnd1
ccnd2
cdkn2a
cdkn2b
cdkn2c
C
RTK/RAS signaling
PDGFRA
PDGFRB
ERBB3
EGFR
ERBB2
FGFR1
FGFR2
MET
GRB2
NF1
NRAS
KRAS
HRAS
ARAF
BRAF
RAF1
SPRY2
D
Epigenetic regulators
Hdac1
Hdac2
Hdac3
Ezh1
Ezh2
Suz12
Eed
Dot1l
jmjd6
Kdm5a
Kdm2b

Suppl. Fig. 1

E13

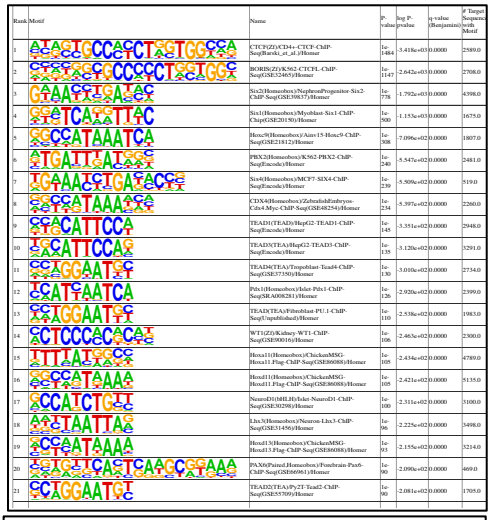

Rank	Motif	Name	P-value	log P-pvalue	q-value (Benjamini)	# Target Sequences with Motif
1		CTCF(Z)/CD4+-CTCF-ChIP-Seq(Barski_et_al.)/Homer	1e-1464	-3.418e+03	0.0000	2589.0
2		BORIS(Z)/K562-CTCFL-ChIP-Seq(GSE32465)/Homer	1e-1147	-2.642e+03	0.0000	2708.0
3		Six2(Homeobox)/NephronProgenitor-Six2-ChIP-Seq(GSE39837)/Homer	1e-778	-1.792e+03	0.0000	4398.0
4		Six1(Homeobox)/Myoblast-Six1-ChIP-Chip(GSE20150)/Homer	1e-500	-1.155e+03	0.0000	1675.0
5		Hoxc9(Homeobox)/Aiolos-Hoxc9-ChIP-Seq(GSE21812)/Homer	1e-308	-7.096e+02	0.0000	1807.0
6		PBX2(Homeobox)/K562-PBX2-ChIP-Seq(Encode)/Homer	1e-249	-5.547e+02	0.0000	2481.0
7		Six4(Homeobox)/MCF7-SIX4-ChIP-Seq(Encode)/Homer	1e-239	-5.509e+02	0.0000	519.0
8		CDX4(Homeobox)/ZebrafishEmbryos-Cdx4-Myc-ChIP-Seq(GSE48254)/Homer	1e-234	-5.397e+02	0.0000	2260.0
9		TEAD1(TEAD)/HepG2-TEAD1-ChIP-Seq(Encode)/Homer	1e-145	-3.351e+02	0.0000	2948.0
10		TEAD3(TEA)/HepG2-TEAD3-ChIP-Seq(Encode)/Homer	1e-135	-3.120e+02	0.0000	3291.0
11		TEAD4(TEA)/Trophoblast-Tead4-ChIP-Seq(GSE77350)/Homer	1e-130	-3.010e+02	0.0000	2734.0
12		Pdx1(Homeobox)/Islet-Pdx1-ChIP-Seq(SRA008281)/Homer	1e-126	-2.920e+02	0.0000	2399.0
13		TEAD(TEA)/Fibroblast-PU.1-ChIP-Seq(Unpublished)/Homer	1e-110	-2.538e+02	0.0000	1983.0
14		WT1(Z)/Kidney-WT1-ChIP-Seq(GSE90016)/Homer	1e-106	-2.463e+02	0.0000	2300.0
15		Hoxa11(Homeobox)/ChickenMSG-Hoxa11.Flag-ChIP-Seq(GSE86088)/Homer	1e-105	-2.434e+02	0.0000	4789.0
16		Hoxd11(Homeobox)/ChickenMSG-Hoxd11.Flag-ChIP-Seq(GSE86088)/Homer	1e-105	-2.421e+02	0.0000	5135.0
17		NeuroD1(bHLH)/Islet-NeuroD1-ChIP-Seq(GSE30298)/Homer	1e-100	-2.311e+02	0.0000	3100.0
18		Lhx3(Homeobox)/Neuron-Lhx3-ChIP-Seq(GSE31456)/Homer	1e-96	-2.225e+02	0.0000	3498.0
19		Hoxd13(Homeobox)/ChickenMSG-Hoxd13.Flag-ChIP-Seq(GSE86088)/Homer	1e-93	-2.155e+02	0.0000	3214.0
20		PAX6(Paired,Homeobox)/Forebrain-Pax6-ChIP-Seq(GSE66961)/Homer	1e-90	-2.090e+02	0.0000	4693.0
21		TEAD(TEA)/Py2T-Tead2-ChIP-Seq(GSE55709)/Homer	1e-90	-2.081e+02	0.0000	1705.0

Core TFs — Six2/Wt1/Hoxd11/TEAD

E16

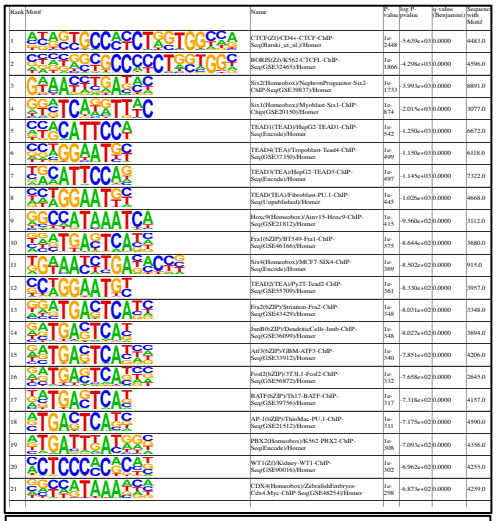

Rank	Motif	Name	P-value	log P-pvalue	q-value (Benjamini)	Sequences with Motif
1		CTCF(Z)/CD4+-CTCF-ChIP-Seq(Barski_et_al.)/Homer	1e-2448	-5.639e+03	0.0000	4483.0
2		BORIS(Z)/K562-CTCFL-ChIP-Seq(GSE32465)/Homer	1e-1866	-4.298e+03	0.0000	4596.0
3		Six2(Homeobox)/NephronProgenitor-Six2-ChIP-Seq(GSE39837)/Homer	1e-1733	-3.993e+03	0.0000	8891.0
4		Six1(Homeobox)/Myoblast-Six1-ChIP-Chip(GSE20150)/Homer	1e-874	-2.015e+03	0.0000	3077.0
5		TEAD1(TEAD)/HepG2-TEAD1-ChIP-Seq(Encode)/Homer	1e-542	-1.250e+03	0.0000	6672.0
6		TEAD4(TEA)/Trophoblast-Tead4-ChIP-Seq(GSE77350)/Homer	1e-499	-1.150e+03	0.0000	6118.0
7		TEAD3(TEA)/HepG2-TEAD3-ChIP-Seq(Encode)/Homer	1e-497	-1.145e+03	0.0000	7322.0
8		TEAD(TEA)/Fibroblast-PU.1-ChIP-Seq(Unpublished)/Homer	1e-445	-1.026e+03	0.0000	4668.0
9		Hoxc9(Homeobox)/Aiolos-Hoxc9-ChIP-Seq(GSE21812)/Homer	1e-415	-9.568e+02	0.0000	3112.0
10		Fra1(bZIP)/BT549-Fra1-ChIP-Seq(GSE46166)/Homer	1e-375	-8.644e+02	0.0000	3680.0
11		Six4(Homeobox)/MCF7-SIX4-ChIP-Seq(Encode)/Homer	1e-369	-8.502e+02	0.0000	915.0
12		TEAD2(TEA)/Py2T-Tead2-ChIP-Seq(GSE55709)/Homer	1e-361	-8.330e+02	0.0000	3957.0
13		Fra2(bZIP)/Striatum-Fra2-ChIP-Seq(GSE43429)/Homer	1e-348	-8.031e+02	0.0000	3348.0
14		JunB(bZIP)/DendriticCells-JunB-ChIP-Seq(GSE36099)/Homer	1e-348	-8.027e+02	0.0000	3694.0
15		Atf3(bZIP)/GBM-ATF3-ChIP-Seq(GSE33912)/Homer	1e-340	-7.851e+02	0.0000	4206.0
16		Fosl2(bZIP)/3T3L1-Fosl2-ChIP-Seq(GSE56872)/Homer	1e-332	-7.658e+02	0.0000	2645.0
17		BATF(bZIP)/Th17-BATF-ChIP-Seq(GSE39756)/Homer	1e-317	-7.318e+02	0.0000	4157.0
18		AP-1(bZIP)/ThioMac-PU.1-ChIP-Seq(GSE21512)/Homer	1e-311	-7.175e+02	0.0000	4590.0
19		PBX2(Homeobox)/K562-PBX2-ChIP-Seq(Encode)/Homer	1e-308	-7.095e+02	0.0000	4356.0
20		WT1(Z)/Kidney-WT1-ChIP-Seq(GSE90016)/Homer	1e-302	-6.962e+02	0.0000	4255.0
21		CDX4(Homeobox)/ZebrafishEmbryos-Cdx4-Myc-ChIP-Seq(GSE48254)/Homer	1e-298	-6.873e+02	0.0000	4259.0

Core TFs + AP-1/BATF

P0-H

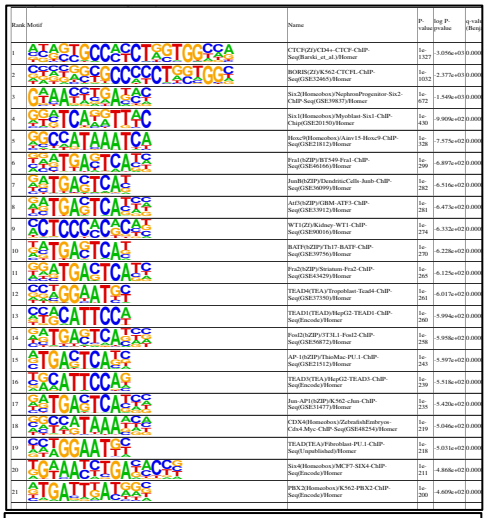

Rank	Motif	Name	P-value	log P-pvalue	q-value (Benj
1		CTCF(Z)/CD4+-CTCF-ChIP-Seq(Barski_et_al.)/Homer	1e-1327	-3.056e+03	0.0000
2		BORIS(Z)/K562-CTCFL-ChIP-Seq(GSE32465)/Homer	1e-1032	-2.377e+03	0.0000
3		Six2(Homeobox)/NephronProgenitor-Six2-ChIP-Seq(GSE39837)/Homer	1e-872	-1.549e+03	0.0000
4		Six1(Homeobox)/Myoblast-Six1-ChIP-Chip(GSE20150)/Homer	1e-430	-9.909e+02	0.0000
5		Hoxc9(Homeobox)/Aiolos-Hoxc9-ChIP-Seq(GSE21812)/Homer	1e-328	-7.575e+02	0.0000
6		Fra1(bZIP)/BT549-Fra1-ChIP-Seq(GSE46166)/Homer	1e-299	-6.897e+02	0.0000
7		JunB(bZIP)/DendriticCells-JunB-ChIP-Seq(GSE36099)/Homer	1e-282	-6.516e+02	0.0000
8		Atf3(bZIP)/GBM-ATF3-ChIP-Seq(GSE33912)/Homer	1e-281	-6.473e+02	0.0000
9		WT1(Z)/Kidney-WT1-ChIP-Seq(GSE90016)/Homer	1e-274	-6.332e+02	0.0000
10		BATF(bZIP)/Th17-BATF-ChIP-Seq(GSE39756)/Homer	1e-270	-6.228e+02	0.0000
11		Fra2(bZIP)/Striatum-Fra2-ChIP-Seq(GSE43429)/Homer	1e-265	-6.125e+02	0.0000
12		TEAD4(TEA)/Trophoblast-Tead4-ChIP-Seq(GSE77350)/Homer	1e-261	-6.017e+02	0.0000
13		TEAD1(TEAD)/HepG2-TEAD1-ChIP-Seq(Encode)/Homer	1e-260	-5.994e+02	0.0000
14		Fosl2(bZIP)/3T3L1-Fosl2-ChIP-Seq(GSE56872)/Homer	1e-258	-5.958e+02	0.0000
15		AP-1(bZIP)/ThioMac-PU.1-ChIP-Seq(GSE21512)/Homer	1e-243	-5.597e+02	0.0000
16		TEAD3(TEA)/HepG2-TEAD3-ChIP-Seq(Encode)/Homer	1e-239	-5.518e+02	0.0000
17		Jun-AP1(bZIP)/K562-cJun-ChIP-Seq(GSE31477)/Homer	1e-235	-5.420e+02	0.0000
18		CDX4(Homeobox)/ZebrafishEmbryos-Cdx4-Myc-ChIP-Seq(GSE48254)/Homer	1e-219	-5.046e+02	0.0000
19		TEAD(TEA)/Fibroblast-PU.1-ChIP-Seq(Unpublished)/Homer	1e-218	-5.031e+02	0.0000
20		Six4(Homeobox)/MCF7-SIX4-ChIP-Seq(Encode)/Homer	1e-211	-4.868e+02	0.0000
21		PBX2(Homeobox)/K562-PBX2-ChIP-Seq(Encode)/Homer	1e-200	-4.609e+02	0.0000

Core TFs + AP-1/BATF

P0-L

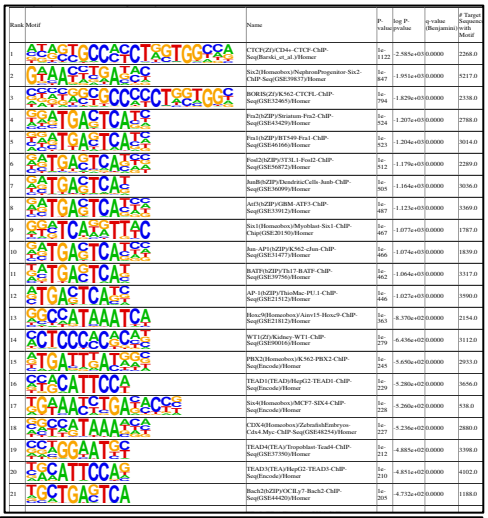

Rank	Motif	Name	P-value	log P-pvalue	q-value (Benjamini)	# Target Sequences with Motif
1		CTCF(Z)/CD4+-CTCF-ChIP-Seq(Barski_et_al.)/Homer	1e-1122	-2.585e+03	0.0000	2268.0
2		Six2(Homeobox)/NephronProgenitor-Six2-ChIP-Seq(GSE39837)/Homer	1e-847	-1.951e+03	0.0000	5217.0
3		BORIS(Z)/K562-CTCFL-ChIP-Seq(GSE32465)/Homer	1e-794	-1.829e+03	0.0000	2338.0
4		Fra2(bZIP)/Striatum-Fra2-ChIP-Seq(GSE43429)/Homer	1e-524	-1.207e+03	0.0000	2788.0
5		Fra1(bZIP)/BT549-Fra1-ChIP-Seq(GSE46166)/Homer	1e-523	-1.204e+03	0.0000	3014.0
6		Fosl2(bZIP)/3T3L1-Fosl2-ChIP-Seq(GSE56872)/Homer	1e-512	-1.179e+03	0.0000	2289.0
7		JunB(bZIP)/DendriticCells-JunB-ChIP-Seq(GSE36099)/Homer	1e-505	-1.164e+03	0.0000	3036.0
8		Atf3(bZIP)/GBM-ATF3-ChIP-Seq(GSE33912)/Homer	1e-487	-1.123e+03	0.0000	3369.0
9		Six1(Homeobox)/Myoblast-Six1-ChIP-Chip(GSE20150)/Homer	1e-467	-1.077e+03	0.0000	1787.0
10		Jun-AP1(bZIP)/K562-cJun-ChIP-Seq(GSE31477)/Homer	1e-466	-1.074e+03	0.0000	1839.0
11		BATF(bZIP)/Th17-BATF-ChIP-Seq(GSE39756)/Homer	1e-462	-1.064e+03	0.0000	3317.0
12		AP-1(bZIP)/ThioMac-PU.1-ChIP-Seq(GSE21512)/Homer	1e-446	-1.027e+03	0.0000	3590.0
13		Hoxc9(Homeobox)/Aiolos-Hoxc9-ChIP-Seq(GSE21812)/Homer	1e-363	-8.370e+02	0.0000	2154.0
14		WT1(Z)/Kidney-WT1-ChIP-Seq(GSE90016)/Homer	1e-279	-6.436e+02	0.0000	3112.0
15		PBX2(Homeobox)/K562-PBX2-ChIP-Seq(Encode)/Homer	1e-245	-5.650e+02	0.0000	2933.0
16		TEAD1(TEAD)/HepG2-TEAD1-ChIP-Seq(Encode)/Homer	1e-229	-5.280e+02	0.0000	3656.0
17		Six4(Homeobox)/MCF7-SIX4-ChIP-Seq(Encode)/Homer	1e-228	-5.266e+02	0.0000	538.0
18		CDX4(Homeobox)/ZebrafishEmbryos-Cdx4-Myc-ChIP-Seq(GSE48254)/Homer	1e-227	-5.236e+02	0.0000	2880.0
19		TEAD4(TEA)/Trophoblast-Tead4-ChIP-Seq(GSE77350)/Homer	1e-212	-4.885e+02	0.0000	3398.0
20		TEAD3(TEA)/HepG2-TEAD3-ChIP-Seq(Encode)/Homer	1e-210	-4.851e+02	0.0000	4102.0
21		Bach2(bZIP)/OCILy7-Bach2-ChIP-Seq(GSE44420)/Homer	1e-205	-4.732e+02	0.0000	1188.0

Core TFs + AP-1/BATF/Bach2

P2

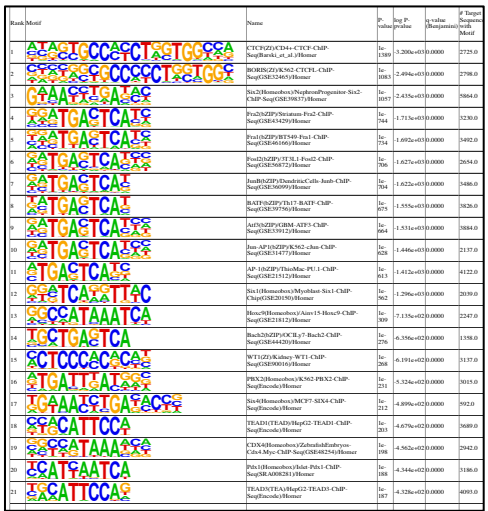

Rank	Motif	Name	P-value	log P-pvalue	q-value (Benjamini)	# Target Sequences with Motif
1		CTCF(Z)/CD4+-CTCF-ChIP-Seq(Barski_et_al.)/Homer	1e-1389	-3.200e+03	0.0000	2725.0
2		BORIS(Z)/K562-CTCFL-ChIP-Seq(GSE32465)/Homer	1e-1063	-2.494e+03	0.0000	2798.0
3		Six2(Homeobox)/NephronProgenitor-Six2-ChIP-Seq(GSE39837)/Homer	1e-1057	-2.435e+03	0.0000	5864.0
4		Fra2(bZIP)/Striatum-Fra2-ChIP-Seq(GSE43429)/Homer	1e-744	-1.713e+03	0.0000	3230.0
5		Fra1(bZIP)/BT549-Fra1-ChIP-Seq(GSE46166)/Homer	1e-734	-1.692e+03	0.0000	3492.0
6		Fosl2(bZIP)/3T3L1-Fosl2-ChIP-Seq(GSE56872)/Homer	1e-706	-1.627e+03	0.0000	2654.0
7		JunB(bZIP)/DendriticCells-JunB-ChIP-Seq(GSE36099)/Homer	1e-704	-1.622e+03	0.0000	3486.0
8		BATF(bZIP)/Th17-BATF-ChIP-Seq(GSE39756)/Homer	1e-675	-1.555e+03	0.0000	3826.0
9		Atf3(bZIP)/GBM-ATF3-ChIP-Seq(GSE33912)/Homer	1e-664	-1.531e+03	0.0000	3884.0
10		Jun-AP1(bZIP)/K562-cJun-ChIP-Seq(GSE31477)/Homer	1e-628	-1.446e+03	0.0000	2137.0
11		AP-1(bZIP)/ThioMac-PU.1-ChIP-Seq(GSE21512)/Homer	1e-613	-1.412e+03	0.0000	4122.0
12		Six1(Homeobox)/Myoblast-Six1-ChIP-Chip(GSE20150)/Homer	1e-562	-1.296e+03	0.0000	2039.0
13		Hoxc9(Homeobox)/Aiolos-Hoxc9-ChIP-Seq(GSE21812)/Homer	1e-309	-7.135e+02	0.0000	2247.0
14		Bach2(bZIP)/OCILy7-Bach2-ChIP-Seq(GSE44420)/Homer	1e-276	-6.356e+02	0.0000	1358.0
15		WT1(Z)/Kidney-WT1-ChIP-Seq(GSE90016)/Homer	1e-268	-6.191e+02	0.0000	3137.0
16		PBX2(Homeobox)/K562-PBX2-ChIP-Seq(Encode)/Homer	1e-231	-5.324e+02	0.0000	3015.0
17		Six4(Homeobox)/MCF7-SIX4-ChIP-Seq(Encode)/Homer	1e-212	-4.899e+02	0.0000	592.0
18		TEAD1(TEAD)/HepG2-TEAD1-ChIP-Seq(Encode)/Homer	1e-203	-4.679e+02	0.0000	3689.0
19		CDX4(Homeobox)/ZebrafishEmbryos-Cdx4-Myc-ChIP-Seq(GSE48254)/Homer	1e-198	-4.562e+02	0.0000	2942.0
20		Pdx1(Homeobox)/Islet-Pdx1-ChIP-Seq(SRA008281)/Homer	1e-188	-4.344e+02	0.0000	3186.0
21		TEAD(TEA)/HepG2-TEAD3-ChIP-Seq(Encode)/Homer	1e-187	-4.328e+02	0.0000	4093.0

Core TFs + AP-1/BATF/Bach2

Suppl. Fig. 2